British Geological Survey

Potential risks of induced seismicity from high volume hydraulic fracturing of shales in Northern Ireland

Multi-Hazards and Risk Programme

Open Report OR/21/003

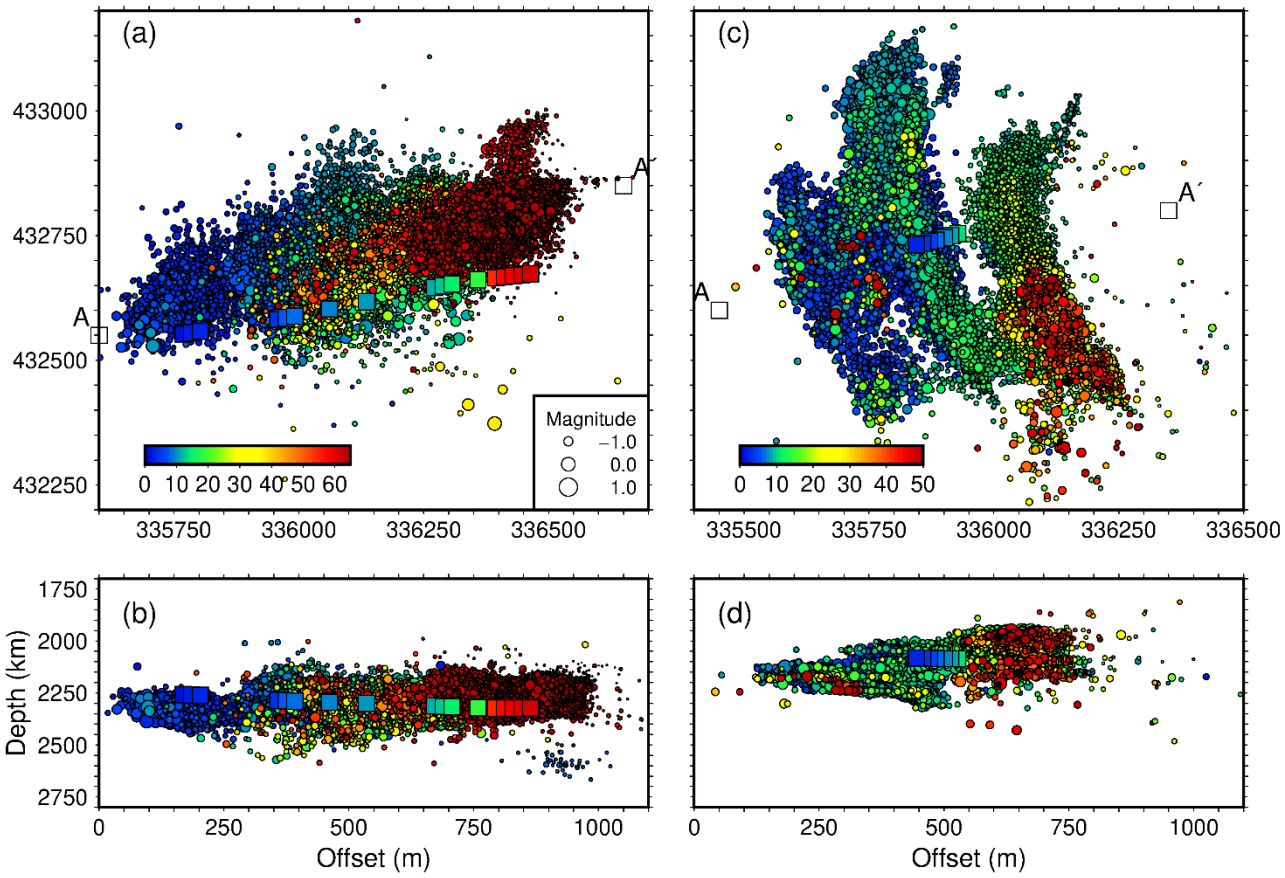

BRITISH GEOLOGICAL SURVEY

MULTI-HAZARDS AND RISK PROGRAMME

OPEN REPORT OR/21/003

Potential risks of induced seismicity from high volume hydraulic fracturing of shales in Northern Ireland

B Baptie and D Reay

Keywords

Earthquakes, pore pressure, stress, faults, hazard, risk.

Front cover

Maps of all events in the microseismic catalogue recorded during operations in PNR-1Z (a) and PNR-2 (c). Events are coloured by time in days from the start of operations and scaled by magnitude. Axes show British National Grid Eastings and Northings. (b) and (d) show depth cross-section showing event depths along the profile A-A´.

Bibliographical reference

BAPTIE, B. & REAY D., 2020. Potential risks of induced seismicity from high volume hydraulic fracturing of shales in Northern Ireland. *British Geological Survey Commissioned Report*, OR/21/003. 46pp.

Keyworth, Nottingham British Geological Survey 2021

BRITISH GEOLOGICAL SURVEY

The full range of our publications is available from BGS shops at Nottingham, Edinburgh, London and Cardiff (Welsh publications only) see contact details below or shop online at www.geologyshop.com

The London Information Office also maintains a reference collection of BGS publications, including maps, for consultation.

We publish an annual catalogue of our maps and other publications; this catalogue is available online or from any of the BGS shops.

The British Geological Survey carries out the geological survey of Great Britain and Northern Ireland (the latter as an agency service for the government of Northern Ireland), and of the surrounding continental shelf, as well as basic research projects. It also undertakes programmes of technical aid in geology in developing countries.

The British Geological Survey is a component body of UK Research and Innovation.

British Geological Survey offices

Nicker Hill, Keyworth,
Nottingham NG12 5GG
Tel 0115 936 3100

BGS Central Enquiries Desk
Tel 0115 936 3143
email enquiries@bgs.ac.uk

BGS Sales
Tel 0115 936 3241
email sales@bgs.ac.uk

The Lyell Centre, Research Avenue South,
Edinburgh EH14 4AP
Tel 0131 667 1000
email scotsales@bgs.ac.uk

Natural History Museum, Cromwell Road,
London SW7 5BD
Tel 020 7589 4090
Tel 020 7942 5344/45
email bgslondon@bgs.ac.uk

Cardiff University, Main Building, Park Place,
Cardiff CF10 3AT
Tel 029 2167 4280

Maclean Building, Crowmarsh Gifford,
Wallingford OX10 8BB
Tel 01491 838800

Geological Survey of Northern Ireland, Department of Enterprise, Trade & Investment, Dundonald House, Upper Newtownards Road, Ballymiscaw,
Belfast, BT4 3SB
Tel 01232 666595
www.bgs.ac.uk/gsni/

Natural Environment Research Council, Polaris House, North Star Avenue, Swindon SN2 1EU
Tel 01793 411500 Fax 01793 411501
www.nerc.ac.uk

UK Research and Innovation, Polaris House,
Swindon SN2 1FL
Tel 01793 444000
www.ukri.org

Website www.bgs.ac.uk
Shop online at www.geologyshop.com

Foreword

The Minerals & Petroleum Branch (MAPB) of the Department for the Economy (DfE) of Northern Ireland, the body responsible for administering petroleum licensing onshore Northern Ireland, asked the Geological Survey of Northern Ireland to carry out a review on the potential risks of induced seismicity from high volume hydraulic fracturing (HVHF) for shale gas or oil, with respect to Northern Ireland. The purpose of the review is to set out the scientific evidence relating to HVHF-related induced seismicity in order to inform the evolving DfE policy on licensing of petroleum exploration and production in Northern Ireland. The potential risk of induced seismicity is only one of many factors that will be taken into consideration by DfE in the development of this policy.

Contents

FIGURES

TABLES

Summary

Hydraulic fracturing (HF) has made it possible to economically produce hydrocarbons directly from low-permeability reservoirs such as shales by injecting high pressure fluids to create fracture networks. However, over the last decade the number of observations of induced earthquakes caused by HF operations around the world has increased as the shale gas industry has developed. Data from the US and Canada suggest that on average around 1% of HF wells can be linked to earthquakes with magnitudes of 3 or greater. Earthquakes of this size are large enough to be felt by people. However, in some areas of the US and Canada the percentage of wells associated with induced earthquakes is much higher (>30%). This variability is often explained in terms of geological factors such as proximity to existing faults. In a small number of cases, HF operations have triggered earthquakes large enough to cause potentially damaging ground motions. Such earthquakes cannot be confidently predicted in advance of operations. These observations suggest that the risk from induced seismicity during HF operations is not negligible.

Earthquakes with magnitudes greater than around 2 result from slip on existing faults that is triggered by stress changes caused by the injection of fluid during the HF process. The size of the earthquake will depend on both the area of the ruptured part of the fault and the amount of slip. Since such faults may extend outside the hydraulically fractured zone, the maximum magnitude will be controlled by local geology and tectonics, not operational parameters such as the amount of injected fluid. As a result, the maximum magnitude is highly uncertain.

Induced earthquakes have been observed in wide variety of geological settings and in areas where there are relatively few tectonic earthquakes. In some areas, the resulting hazard from induced earthquakes due to HF operations is significantly greater than the hazard from tectonic earthquakes. As a result, the low hazard from tectonic earthquakes in Northern Ireland does not guarantee that the hazard from induced seismicity will also be low.

Induced earthquakes are likely to be clustered in space and time around the locus of HF operations. Hazard is likely to increase with the number of wells and will be highest during or shortly after HF operations. Hazard may also be a function of total injected volume, with larger injected volumes leading to more earthquakes and increasing the probability of larger events. Operations that target shallow formations may pose a higher hazard, since for a given magnitude, the intensity of ground motions at the surface will be greater. The potential for actual damage depends on the intensity of motions and both the number and vulnerability of buildings exposed to ground shaking. As a result, the risk of damage to buildings will be higher in densely populated urban areas than in rural areas. Risk studies for the UK have shown that cosmetic and minor structural damage may occur for earthquakes with magnitudes as low as 3.

Higher resolution geophysical data is needed to identify fault structures and depth to basement in sedimentary basins with hydrocarbon potential in Northern Ireland in order to help mitigate risk of induced seismicity from hydraulic fracturing. Improved regional seismic monitoring should also be considered. Similarly, the present-day stress regime and stress state of faults in both the Lough Allen and Rathlin basins is poorly known. Further work is needed to address this.

Current risk-mitigation strategies have had limited success. There may be insufficient data to identify geological faults prior to operations and even where high resolution data are available, there may still be hidden faults. Similarly, traffic light systems based on specific earthquake magnitude thresholds have often failed. Statistical methods that relate the volume of injected fluid or the injection rate to induced earthquake activity may allow useful probabilistic forecasts in the future but may be associated with considerable uncertainties without calibration for local conditions.

1 Introduction

The Minerals & Petroleum Branch (MAPB) of the Department for the Economy (DfE) of Northern Ireland, the body responsible for administering petroleum licensing onshore Northern Ireland, asked the Geological Survey of Northern Ireland to carry out a review on the potential risks of induced seismicity from high volume hydraulic fracturing (HVHF) for shale gas or oil, with respect to Northern Ireland. The purpose of the review is to set out the scientific evidence relating to HVHF-related induced seismicity in order to inform the evolving DfE policy on licensing of petroleum exploration and production in Northern Ireland. The potential risk of induced seismicity is only one of many factors that will be taken into consideration by DfE in the development of this policy.

It is relatively well-known that anthropogenic activity can result in man-made or "induced" earthquakes. Although such events are generally small in comparison to natural earthquakes, they are often perceptible at the surface and some have been quite large. Underground mining, deep artificial water reservoirs, oil and gas extraction, geothermal power generation and waste disposal have all resulted in cases of induced seismicity. A number of prior review articles and reports have addressed this issue (e.g., McGarr *et al*., 2002; Davies *et al*., 2013; Ellsworth 2013; National Research Council 2012; Grigoli *et al*., 2017; Keranen and Weingarten, 2018). These activities all have the potential to change the state of stress, which can induce or trigger slip on faults within the Earth. The connection between human activity and induced seismicity is usually based on both a spatial and temporal coincidence, although this is not always clear.

Schultz *et al*. (2020) summarise the current state of knowledge of induced seismicity associated with hydraulic fracturing for shale gas and presents some well-documented case studies, as well as identifying areas for further research. Another recent review by Atkinson *et al*. (2020) concluded that hydraulic fracturing can trigger earthquakes large enough to cause potentially damaging ground motions and that the hazard from earthquakes induced by hydraulic fracturing might greatly exceed the natural earthquake hazard in regions of low to moderate seismicity.

In a more regional context, reviews commissioned by the UK Government (Royal Society, 2012) and the Environmental Protection Agency (EPA) of Ireland (Hooper *et al*., 2016) considered the wider risks (including induced seismicity) associated with hydraulic fracturing to extract shale gas in the UK and Ireland, respectively. Both these studies concluded that the risk of induced seismicity was low. Following the seismicity induced by the first hydraulic fracturing of a shale gas reservoir in the UK, the Oil & Gas Authority commissioned Green *et al*. (2012) to review the activity and suggest measures for future mitigation. A study commissioned by the Scottish Government (Baptie *et al*., 2016) considered the levels of induced seismic activity that could be associated with unconventional oil and gas activities in Scotland and the regulatory and non-regulatory actions that could be taken to mitigate risks. The current review draws on the findings of these and other reviews and applies them to the relevant geological settings in Northern Ireland.

Specifically, this review addresses the following questions:

- What is the process of high-volume hydraulic fracturing and how is it used to extract shale oil and gas?
- What is the global experience of induced seismicity resulting from the shale oil and gas industry in general and hydraulic fracturing (HF) in particular? What are the characteristics of HF-induced seismicity?
- What do we know about the triggering mechanisms for induced seismicity and what make some areas susceptible and others not?
- What is the natural seismicity of Ireland and how might this relate to the risks of induced seismicity?
- How might the structural geology of the sedimentary basins in Northern Ireland with shale gas resource potential impact the induced seismicity hazard?

- What can we say about the hazards and risks of induced seismicity from HF given the global experience to date?
- What mitigation measures can be used to reduce the risks of and from induced seismicity and how successful are they?

The information is then drawn together to give an assessment of the risk from the induced seismicity hazard in Northern Ireland, including the scientific uncertainties and data gaps that limit our knowledge of the subject. This review also recognises that perception of risk in the community may be equally or more important than the quantifiable risk from induced seismicity but this topic is outside the scope of the review.

2 Hydraulic fracturing of shale reservoirs

While it has long been recognised that many source rocks such as shales still contained significant amounts of hydrocarbons, these were widely considered uneconomical because of their low permeability. The advent of hydraulic fracturing (HF) has made it possible to economically produce hydrocarbons directly from these low-permeability formations, unlocking their vast reserves and transforming the industry over the last decade or so. In this process, fluid is pumped into the subsurface at high pressure, increasing pore pressure until it exceeds the pressure needed to create new fractures in the rock. This causes hydraulic fractures and shear failures propagate throughout the rock matrix (e.g., Detournay, 2016), creating a permeable fracture network that allows fluids to flow into the well bore. Accompanying technological advances such as horizontal drilling and the use of proppants such as sand or aluminium oxide to hold fractures open (Liang *et al.*, 2016), and the addition of heavy-molecular-weight polymers to the injected water to reduce drag and reduce energy demand (Palisch *et al*., 2010) have increased yields of oil and gas from wells and led to the USA becoming the largest global oil producer in 2019.

Figure 1 shows a schematic with the main elements of the process. Multiple wells may be drilled from a single well pad and HF is carried out at discrete points along the horizontal section of

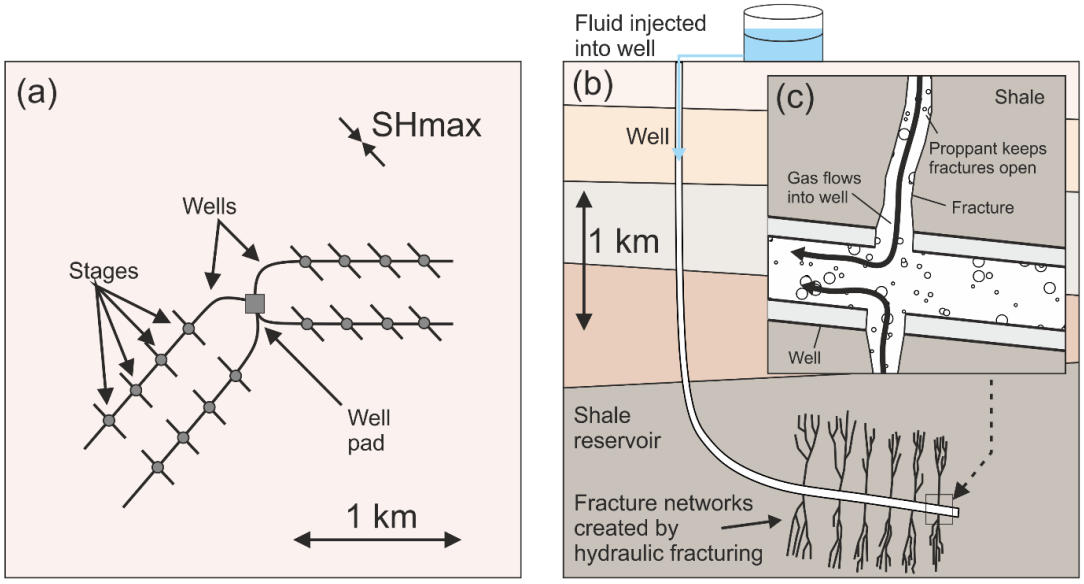

Figure 1. Schematic showing the main elements of the hydraulic fracturing processing. (a) Plan view showing four lateral wells from a single well pad (grey square) each with four HF stages (grey circles). Fractures are expected to open parallel to the maximum horizontal compressive stress (SHmax). (b) Depth section. During each stage, fluid is pumped into the well at high pressure, increasing pore pressure in the reservoir creating a permeable fracture network. (c) Detailed section showing facture held open by proppant allowing fluid to flow into the well bore. Distances are indicative.

each well, commonly referred to as stages. Each stage may take several hours and a well may be fracked over a matter of days or weeks. When all the fracture stages have been completed most of the frack fluid may return up the well to the surface as 'flowback' and, at least in the early stages of production, formation water may also come up as produced fluids. Typically, the initial flow rate from an individual well may be high but it drops off exponentially so that an increasing number of wells need to be drilled to maintain production volumes over many years.

There have been widespread concerns regarding the environmental impacts of the technique, aside from the possibility of earthquakes induced directly by operations. For example, the large number of wells and the need for large volumes of water has led to concern about both groundwater contamination (Myers, 2012) and overuse of water resources (Chen & Carter, 2016). Similarly, the management and subsurface disposal of large volumes of produced brines has also led to fears of both contamination (Gregory *et al*., 2011) and the potential for induced earthquakes (e.g., Ellsworth, 2013). Finally, the escape of methane, a potent greenhouse gas, as well as the wider need to reduce the greenhouse gas emissions are also widely cited as arguments against hydraulic fracturing. These factors have provoked strong opposition to the exploitation of such 'unconventional' shale reservoirs, with many countries imposing moratoria or outright bans on high volume hydraulic fracturing of shales.

3 Global experience of induced seismicity associated with the shale oil and gas industry

The process of hydraulically fracturing a borehole, as implemented for shale gas recovery, has previously been considered to pose a low risk of inducing either felt, damaging or destructive earthquakes (e.g., National Research Council, 2012; Royal Society and Royal Academy of Engineering, 2012). In the US, where ~1.8 million hydraulic fracturing operations have been carried out in ~1 million boreholes (Gallegos and Varela, 2014), there are relatively few published cases of HF induced earthquakes that were large enough to have been widely felt. Atkinson *et al*. (2016) states that only ~0.3% of horizontally drilled HF wells in the Western Canada Sedimentary Basin (WCSB) are associated with earthquakes with magnitudes greater than 3.0 Mw. Ghofrani and Atkinson (2016) suggest that the probability of earthquakes with M ≥ 3 within a 10 km radius of HF wells in the WCSB is 0.010 to 0.026. However, there are an increasing number of published examples of earthquakes in unconventional shale development areas worldwide that have been strongly felt, and, in some cases, caused damage (Schultz *et al*, 2020; Atkinson, 2020). Some of the most notable examples are shown in Figure 2 and listed in Table 1. These include documented cases from the USA (Oklahoma, Texas, Ohio), Canada (Alberta, BC), the UK and China. In this section, we present a summary of these cases. For a more detailed discussion of these, we refer the reader to Schultz *et al*. (2020) and the references therein.

The first documented example of larger earthquakes induced by HF operations was in the Horn River Basin, which lies across the border between the Northwest Territories and British Columbia (BC), Canada, and is one of the largest shale gas plays in North America. Thirty-eight earthquakes were detected by the regional seismic monitoring network between 8/4/2009 and 13/12/2011 (BC Oil and Gas Commission, 2012). Twenty-one of the earthquakes had magnitudes of 3.0 or greater, and the largest event had a magnitude of 3.8 M_L. This event was also felt by workers in the area.

The Exshaw Formation in southern Alberta has undergone limited unconventional development, however, more than 60 small earthquakes (up to 3.0 M_L) were detected from December 2011 to March 2012 north of Cardston, Alberta during HF operations (Schultz *et al*., 2015). This area had no prior documented seismic activity of comparable magnitude or frequency. The first four stimulations were aseismic whereas the following six resulted in earthquakes.

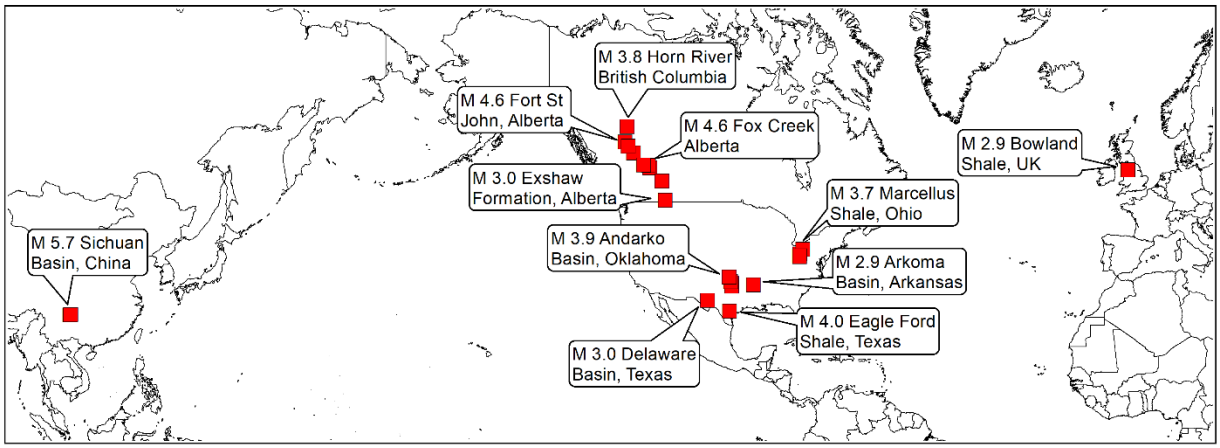

Figure 2. Global distribution of notable earthquakes induced by hydraulic fracturing (HF). This includes documented cases from the USA (Oklahoma, Texas, Ohio), Canada (Alberta, BC), the UK and China [see Data and Resources for earthquake data].

The Duvernay Formation in the Alberta Basin contains vast resources of shale oil and gas. Development of the play began in 2010 and the first reported cases of induced seismicity in 2013 occurred near the town of Fox Creek (Schultz *et al*., 2015; Schultz *et al*., 2017). Almost 200 events with magnitudes of 2.0 M_L or greater have been induced by HF operations in this basin. The largest of these was a magnitude 4.6 *Mw* earthquake in 2015 (Schultz *et al.*, 2017). No injuries or property damage were linked to this earthquake and the recorded ground motions were below the levels typically observed to cause damage to structures. However, the event triggered an automatic shutdown of a nearby gas plant and precautionary flaring of gas.

The Montney Formation that spans the border between BC and Alberta in western Canada is considered one of the most productive hydrocarbon plays in North America and there have been more than 7,000 HF wells completed in the formation from 2007–2020. Induced seismicity here has led to a significant change in the regional seismicity rate and around 100 events with magnitudes of 2.0 M_L or greater have been induced by HF operations. The largest event was observed on 17 August 2015 in the northern Montney area with a magnitude of 4.6 *Mw* (Babaie Mahani *et al*., 2017, 2019).

Oklahoma in the United States is more commonly associated with earthquakes induced by waste-water disposal, with dramatic increases in induced seismicity as a result of long-term disposal of large volumes of waste-water from both conventional and unconventional hydrocarbon production in deep boreholes (Ellsworth, 2013; Rubenstein and Mahani, 2015; Walsh and Zoback, 2016). However, induced seismicity induced by HF has also been observed in both the SCOOP and STACK plays of the Anadarko Basin. Two of the first examples were magnitude 2.9 M_L and 3.2 M_L earthquakes in 2011 and 2014 in Garvin and Carter Counties, respectively (Holland, 2013; Darold *et al*., 2014). More recently, Skoumal *et al*., 2018a) identified 274 HF wells correlated to seismicity, with the largest a magnitude 3.5 M_L event on 14 July 2015. A further 960 earthquakes with $M_L \geq 2$ were linked to HF between 2016 and 2019, with the largest a magnitude 3.9 M_L event on 25 July 2019 in Kingfisher County.

The Utica and Marcellus Shales of the northern Appalachian Basin in the eastern United States are some of the most developed unconventional plays in the world. with more than 11,000 HF wells completed since 2009. This coincided with a significant increase in seismicity rate linked to both waste-water disposal and HF. The earliest reported case of HF-induced seismicity was in Harrison County with a magnitude 2.1 M_L earthquake in 2014 (Friberg *et al*., 2014). Another early example was a magnitude 3.0 ML earthquake near Poland Township (Skoumal *et al*., 2015a). The largest recorded event linked to HF in the basin was a magnitude 3.7 M_L earthquake in Noble County, 2017.

There have been more than 19,000 HF wells completed in the Eagle Ford Shale play in South Texas along with significant increases in seismicity rates. Fasola *et al*. (2019) found that more

than 85% of the seismicity in the play and 94 earthquakes with magnitudes greater than 2.0 M_L was correlated with HF. A magnitude 4.0 Mw earthquake on 1 May 2018 earthquake is the largest HF-induced earthquake documented in the United States.

At least 7,900 HF wells have been completed in the Delaware Basin, Texas, from 2011–2019, where the Bone Spring and Wolfcamp formations contain significant reserves of unconventional oil and gas. Seismicity rates have increased significantly over the past decade, although most of the earthquake activity is thought to have been by wastewater disposal. Skoumal (2020) suggests that only 5% of seismicity was induced by HF. The largest of these was a magnitude 3.0 M_L event in May 2018.

Lei *et al*. (2017) report that since the start of hydraulic fracturing operations in December 2014, there have been rapid increases in seismicity at the Shangluo shale gas site in the Sichuan Basin, China. The authors provide evidence to suggest that earthquakes with moment magnitudes up to 4.7 Mw were caused by injection-induced fault reactivation. Lei *et al*. (2017) also suggest that the number of induced earthquakes is so high in this area because of: (1) strong and brittle Pre-Triassic sedimentary rocks; (2) critical regional stress; (3) widely existing faults; (4) insufficient top and bottom seals and/or no fracturing barrier between the shale formation and the rocks above and below.

A magnitude 5.7 M_L earthquake struck Xingwen County, Sichuan Province, China, on 16 December 2018. A few weeks later, on 3 January 2019, a magnitude 5.3 M_L earthquake occurred 8 km to the west. These were the largest and most damaging events in the Changning shale gas block and resulted in extensive damage to nearby farmhouses and other structures. Lei *et al*. (2019) provide evidence to suggest that the events were induced by nearby hydraulic-fracturing operations at depths of 2.5-3 km. This evidence includes a strong correlation in both space and time to operations, the statistical behavior of the seismicity, and the estimated overpressure required to activate faults that are unfavourably oriented with respect to the regional stress field.

In 2011, HF of the first dedicated shale gas well in the UK, Preese Hall 1 (PH-1) near Blackpool, Lancashire, led to felt seismicity (Clarke *et al*., 2014), the suspension of HF operations, and inquiries into induced seismicity and risks (de Pater and Baisch 2011; Royal Society and Royal Academy of Engineering, 2012). The largest seismic event, on 1 April 2011, had a magnitude of 2.3 M_L and was felt locally at an intensity of 4 EMS (European Macroseismic Scale (Grünthal, 1998)). De Pater and Baisch (2011) concluded that the earthquake activity was caused by fluid injection directly into a nearby fault zone, which reduced the effective normal stress on the fault and caused it to fail repeatedly in a series of small earthquakes.

In late 2018, HF of the Bowland Shale in the PNR-1z well was carried out at Preston New Road, Blackpool. Operations in the PNR-1Z well were accompanied by seismicity and the largest event, with a magnitude of 1.6 M_L, was felt by a small number of people near the epicentre. HF operations in the adjacent PNR-2 well started on 15 August 2019 and were also accompanied by seismicity. The largest of these events had a magnitude of 2.9 M_L and occurred on 26 August 2019 at 07:30 UTC, almost 72 hours after the last HF stage on 23 August. The earthquake was strongly felt at distances of up to a few kilometres from the epicenter with maximum intensities of 6 EMS and led to a premature end to operations in the PNR-2 well with only 7/47 HF stages completed. The UK government subsequently announced an immediate moratorium on HF due to the possibility of unacceptable impacts on local communities.

Country	Region	Formation or Play	Age	Number of wells	Year(s)	Maximum magnitude	Significant geological factors & faulting mechanisms	Traffic Light System
Canada	Horn River Basin, BC	Muskwa Shale	DEV	11+	2009-11	Up to 3.8		NO
Canada	Alberta Basin	Exshaw	DEV - CARB	~40 HF wells	2011-12	Up to 3.0	Palaeokarst adjacent to basement-rooted fault	NO
Canada	Alberta Basin	Duvernay	DEV	1000 HF wells	2013-19	Up to 4.4	Basement-rooted transtensional strike-slip faults	Y: 1.0 R: 3.0
Canada	AB/BC	Montney	TRIAS	>7000 HF wells	2006-20	2.4 – 4.6	Reverse and strike-slip mechanisms	R: 4.0
USA	OH, PA, VA	Marcellus & Utica	DEV - CARB	>1100 HF	2013 -	Up to 3.7	Previously unmapped linear strike-slip fault segments	Y: 2.5 R: 3.0
USA	OK; Anadarko & Arkoma Basins	SCOOP & STACK	DEV - CARB	>13000 HF wells	2013 -	Up to 3.9	Injection into dolomitic carbonates near basement. Strike-slip faulting	Y: 2.5 R: 3.5
USA	AR;	Fayetteville	CARB	>1000 HF wells	2004-09; 2010-11	Up to 2.9	Activation of strike-slip basement faulting.	No.
USA	TX;	Eagle Ford	CRET	>19000 HF		Up to 4.0	Normal faulting	NO
USA	TX, NM: Delaware Basin	Wolfcamp & Bone Spring	PERM	>7900 HF wells (TX)	2010 -	Up to 3.0		NO
China	South Sichuan Basin	Wufeng - Longmaxi	ORD - SIL	>500 HF wells	2014 -	Up to 5.7	Reverse or strike slip movement in dolomitic strata between target and basement	NO
UK	LANC	Bowland	CARB	2 HF wells	2011; 2018-19	2.3; 1.6, 2.9	Fluid injection directly into fault	Y: 0.5 R: 2.0

Table 1. Summary of documented cases of hydraulic fracturing induced seismicity reviewed by Schultz *et al*. 2020. CRET Cretaceous, TRIAS Triassic, PERM Permian, CARB Carboniferous, DEV Devonian; SIL Silurian; ORD Ordovician. HF Hydraulic fracturing; WWI wastewater injection. Y: yellow or orange; R: red.

4 Key features

In this section we examine some of the key features of seismicity induced by HF that are important for subsequent understanding of the hazard and how these features may be influenced by operational parameters.

4.1 FREQUENCY OF OCCURRENCE

Despite huge numbers of HF operations in wells in different basins across the US and western Canada, only a relatively small percentage of wells can be linked of earthquake activity. Some basins show no cases of induced seismicity at all despite similar amounts of HF activity and in basins where there is induced seismicity associated with HF, it is often associated with some wells but not others.

In the US, where ~1.8 million hydraulic fracturing operations have been carried out in ~1 million boreholes (Gallegos and Varela, 2014), there are relatively few published cases of HF induced earthquakes that were large enough to have been widely felt (e.g., Holland, 2013; Friberg *et al*., 2014; Skoumal *et al*., 2015a). Skoumal *et al*. (2015b) used data from regional seismic networks to estimate the fraction of HF wells associated with induced seismicity in Ohio, finding that approximately ~0.35% of ~850 unconventional wells had induced seismicity large enough to be detected (M >2). Further analysis in Ohio by Brudzinski and Kozłowska (2019) increased this to ~2.7%. In Pennsylvania and West Virginia, induced seismicity was associated with ~0.05% and ~0.3% of HF wells, respectively (Skoumal *et al*., 2018b; Brudzinski and Kozłowska, 2019). Skoumal *et al*. (2018a) found that ~1.8% of 12,000 HF wells in Oklahoma between 2010 and 2016 were correlated with seismicity.

Atkinson *et al*. (2016) found that only ~0.3% of horizontally drilled HF wells in the Western Canada Sedimentary Basin (WCSB) were associated earthquakes with magnitudes greater than 3.0 Mw. Ghofrani and Atkinson (2016) develop a statistical model of the likelihood that horizontally fractured wells in the WCSB will trigger earthquakes with $M \geq 3$ and map how that likelihood varies spatially (Figure 3). The results show that from 14,046 HF wells with multistage hydraulic fracture treatments, the regional average probability of earthquakes with M ≥ 3 within a 10 km radius of a HF well is 0.010 to 0.026.

However, in some areas the percentage of wells associated with induced earthquakes can be much higher. Schultz *et al*. (2018) found that ~15% of HF wells within the Kaybob region of the Duvernay play (Alberta) were associated with induced seismicity. Kozłowska and Brudzinski (2018) found that between 10% and 33% of HF wells in four ~20 × 20-km regions of Ohio had induced earthquakes. Skoumal *et al*. (2018) finds comparable ratios in four regions in Oklahoma. Shemeta *et al*. (2019) found that 7.7% of HF wells in Oklahoma were associated with earthquakes of $M_L \geq 2$, with rates as high as 19.5% in some areas. In the Bowland Shale (UK), HF operations have only occurred in three wells, but these have produced events with maximum magnitudes of M = 2.3, 1.6 and 2.9 respectively(Clarke *et al*., 2014; Clarke *et al*., 2019).

4.2 PROXIMITY TO THE WELL

The majority of HF-induced earthquakes with well-constrained locations tend to be close to the well pad where HF has taken place (Skoumal *et al*., 2020). In a number of cases, seismicity is observed to lie on linear fault structures that are within a few hundreds of meters of lateral sections of the well (e.g., Eyre *et al*., 2019a). These distances seem consistent with the expected sizes of fracture systems stimulated by operations that might connect with existing faults and increase fault pore pressure toward failure (Shen *et al*., 2019). This is also consistent with a lack of wider pore pressure diffusion due to the low permeability of the reservoir.

However, in other cases the separation between well and seismicity is greater. For example, earthquakes observed at Cardston, Alberta (Schultz *et al*., 2015) and Poland Township, Ohio cases (Skoumal *et al*., 2015a) were located 1 km below the target formation, within the

crystalline basement. Similarly, induced seismicity in both the Kaybob Duvernay (Bao & Eaton, 2016) and Red Deer, Alberta (Schultz & Wang, 2020) was laterally offset from the nearest HF stage by 1.0 and 1.5 km, respectively, well beyond the plausible extent of HF growth (Davies *et al*., 2012).

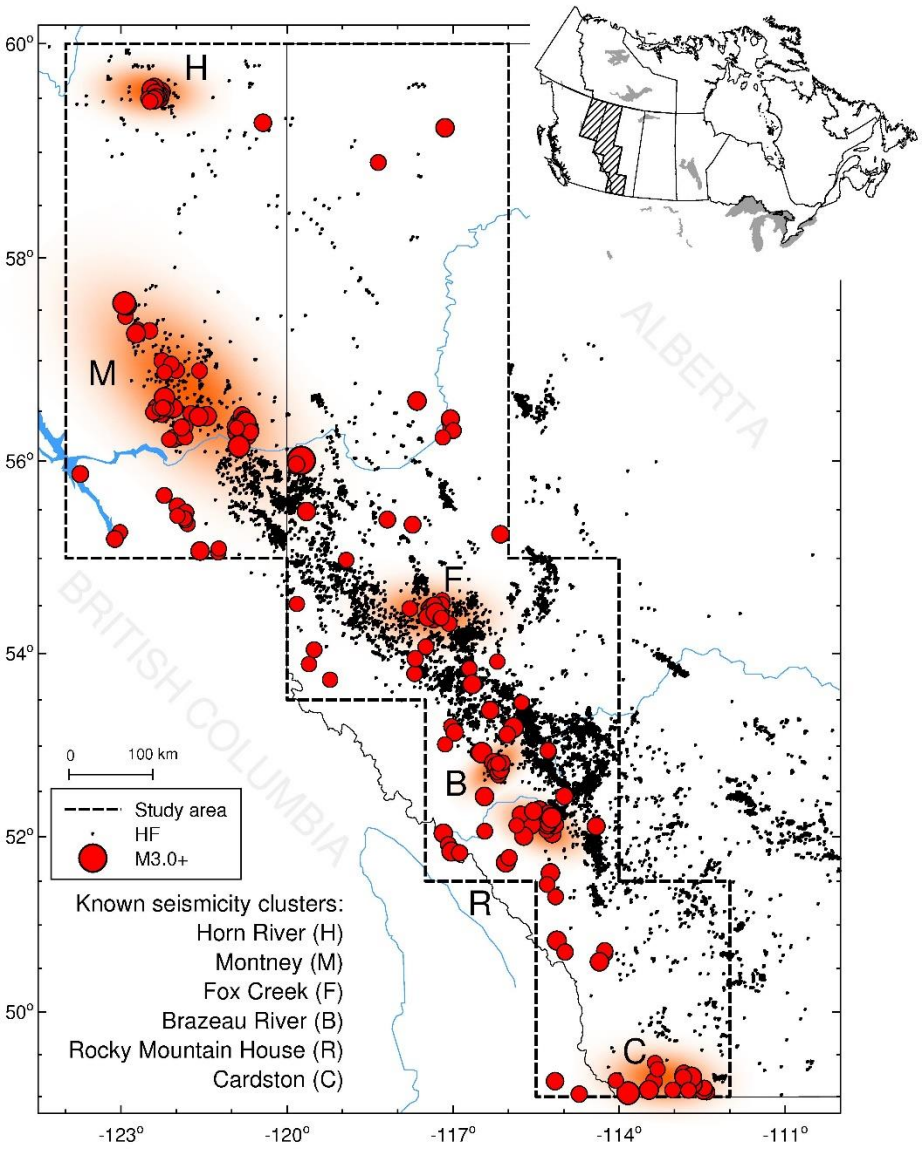

Figure 3. Seismicity and wells database for the WCSB from Ghofrani & Atkinson (2016). Events of moment magnitude M≥3 are shown since 1985 (red circles), from the Canadian Composite Seismicity Catalogue (www.inducedseismicity.ca); all non-earthquake events (e.g. blasts) have been removed. Hydraulic fracture (HF) wells are shown with black dots. Well data obtained from the Alberta Energy Regulator [https://www.aer.ca/data-and-publications] and the B.C. Oil and Gas Commission [http://data.bcogc.opendata.arcgis.com]. Earthquake data from the Canadian Composite Seismicity Catalogue [https:// www.inducedseismicity.ca].

4.3 TEMPORAL RELATIONSHIP WITH OPERATIONS

HF induced seismicity typically shows a rapid response to stimulation with earthquake rates peaking during periods of injection. Schultz *et al*. (2018) suggest that up to 90% of induced events occur during stimulation. In some cases, seismicity clearly correlates with individual HF stages. For example, Clark *et al.* (2019), Eaton *et al*. (2018), Schultz *et al.* (2015) and Yu *et al*. (2019). Figure 4 shows histograms of the number of events during each stage along with the injected volume of fluid during HF of the PNR-1z well at Preston New Road, Lancashire. Event rates are observed to increase as soon as injection starts and generally reach a peak towards

the end of the period of injection. After injection stops, the rates decay quickly over the subsequent hours. Histograms for those stages that show more complex injection histories, e.g., stages 22 and 30, also show multiple peaks in activity rate that correlate with the observed periods of injection.

In other cases, a delay of several hours can be observed between stage stimulation and the largest earthquakes (Kettlety *et al*., 2019; Kwiatek *et al*., 2019). The largest earthquakes during operations at Preese Hall, Lancashire, UK (Clark *et al*, 2014) occurred approximately eight hours after injection stopped, while the well was shut-in and under high pressure. Similarly, the two largest events during operations in the PNR-2 well at Preston New Road, Lancashire, UK, with magnitudes of 2.1 and 2.9 M_L occurred approximately 40 hours and 72 hours after the last HF stage.

Earthquake rates typically return to background levels within a few days of the cessation of operations, although in some cases rates have remained elevated for months (Atkinson *et al*., 2016; Ghofrani & Atkinson, 2020; Kozłowska *et al*., 2018). However, some of the largest magnitude events have occurred after completion of HF operations (Meng *et al*., 2019; Schultz *et al*., 2017).

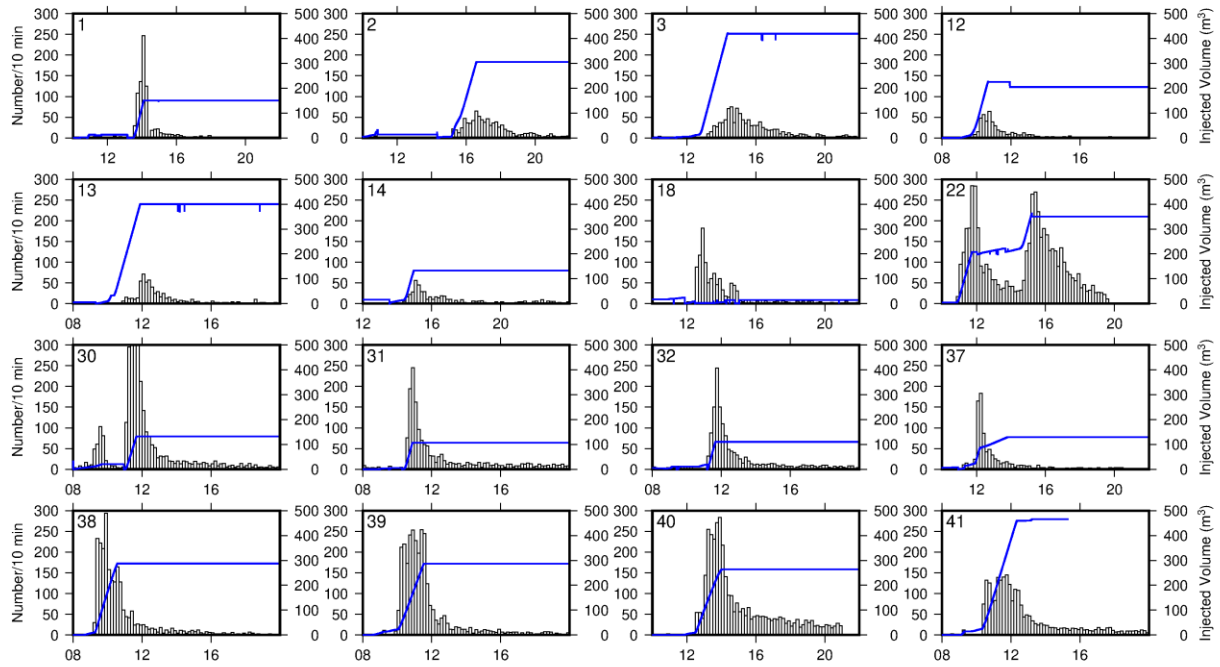

Figure 4. Histograms showing the number of events in 10 minutes windows as a function of time during injection into various stages of the PNR-1z well, Preston New Road, Lancashire. Blue lines show the cumulative volume of injected fluid during hydraulic fracturing operations. The number in the top left of each plot is the stage number. Operational data from the Oil and Gas Authority [available at https://www.ogauthority.co.uk/exploration-production/onshore/onshore-reports-and-data/].

4.4 RELATIONSHIP WITH INJECTED VOLUME

The cumulative volume of injected fluid is often considered to be an important factor in controlling earthquake rate in some areas susceptible to HF-induced earthquakes. For example, Schultz *et al*. (2018) found that injection volume was the key operational parameter correlated with induced earthquakes in the Duvernay Formation in the Alberta Basin, Canada. In the Horn River Basin (British Columbia) large seismic-moment release only occurred when the total monthly injected volume, across the basin, exceeded 150,000m^3 (Farahbod *et al*., 2015). In other areas, such as the Eagle Ford play in Texas, the volume of injected fluid per unit area per

day was seen to be an important factor in the rate of induced seismicity associated with HF (Fasola *et al*., 2019).

McGarr (2014) suggested that both the maximum magnitude and the total seismic moment released of earthquakes induced by fluid injection were limited by the total volume of injected fluid. Figure 5 (a) shows total seismic moment release for a number of examples of induced seismicity as a function of injected volume in HF, Enhanced Geothermal System (EGS) and waste water disposal from McGarr (2014) Table 1. The red and green crosses show PNR-1z and PNR-2. These are quite different despite similar injected volumes into two wells less than a few hundred meters apart and into the same geological unit. Although less fluid was injected into the PNR-2 well, more seismic moment was released. This may suggest that in this case local heterogeneities in the pre-existing stress field partially determine seismicity. Figure 5 (b) and (c) show both seismic moment release and the number of recorded events for each HF stage during operations in PNR-1z and PNR-2. In the case of PNR-2, the in-stage moment release does not include the largest events, which occurred days after operation stopped.

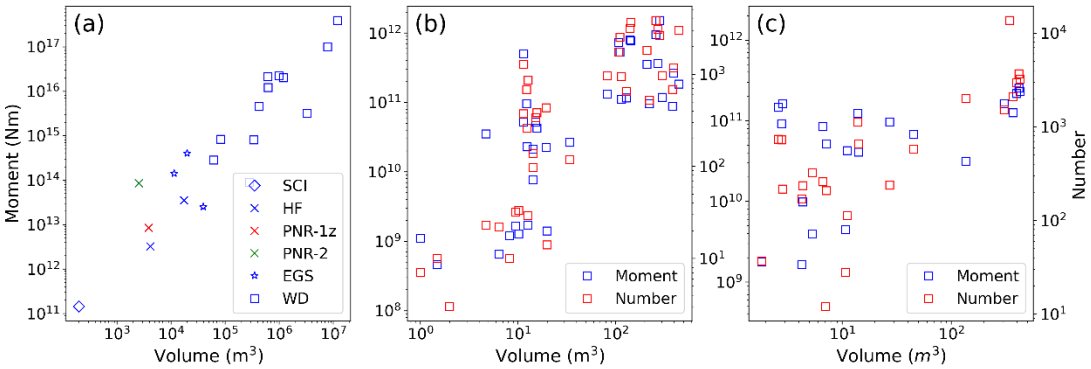

Figure 5. (a) Total seismic moment release as a function of injected volume in HF, EGS and waste water disposal from McGarr (2014) Table 1 as well as data from the PNR-1z (red cross) and PNR-2 (green cross) wells at Preston New Road. (b) and (c) show cumulative seismic moment for each HF stage at PNR-1z and PNR-2 respectively, as a function of the injected volume for that stage. Operational data from Preston New Road published by the Oil and Gas Authority [available at https://www.ogauthority.co.uk/exploration-production/onshore/onshore-reports-and-data/].

Induced seismicity is also observed in basins where there are only limited numbers of wells and relatively small injection volumes. For example, Preese Hall-1, near Blackpool, was the first shale gas exploration well in the UK and there were six HF stages in this vertical well (Clarke *et al*., 2014). Induced seismicity was associated with Stages 2 and 4 (with the largest injected volumes) but Stages 1, 3 and 6 (with smaller volumes) were aseismic and Stage 5, where flowback took place, only weakly seismic. Similarly, the M 5.5 earthquake induced at an EGS at Pohang, South Korea, is a clear exception, with only 1/500 of the injected volume predicted by the McGarr (2014) model for an earthquake of this magnitude (Ellsworth *et al*., 2019).

5 Triggering Mechanisms

While microseismic events related to the creation of fracture networks in an impermeable shale reservoir are considered a normal part of HF operations, disruptive or even damaging induced earthquakes require the activation of pre-existing fault systems. This requires operations to cause a stress perturbation that is sufficient to trigger slip on a fault. In general, the stress change required to reactivate a fault will depend on the in-situ stress field and the orientation of the fault and slip is most likely to occur for critically stressed faults that are already close to failure and only require a small stress change to allow reactivation. In this section we discuss three of proposed mechanisms by which HF operations could trigger slip on existing faults: pore

pressure increases; poroelastic stress transmission; and, pore pressure causing aseismic slip. These are shown graphically in the schematic in Figure 6.

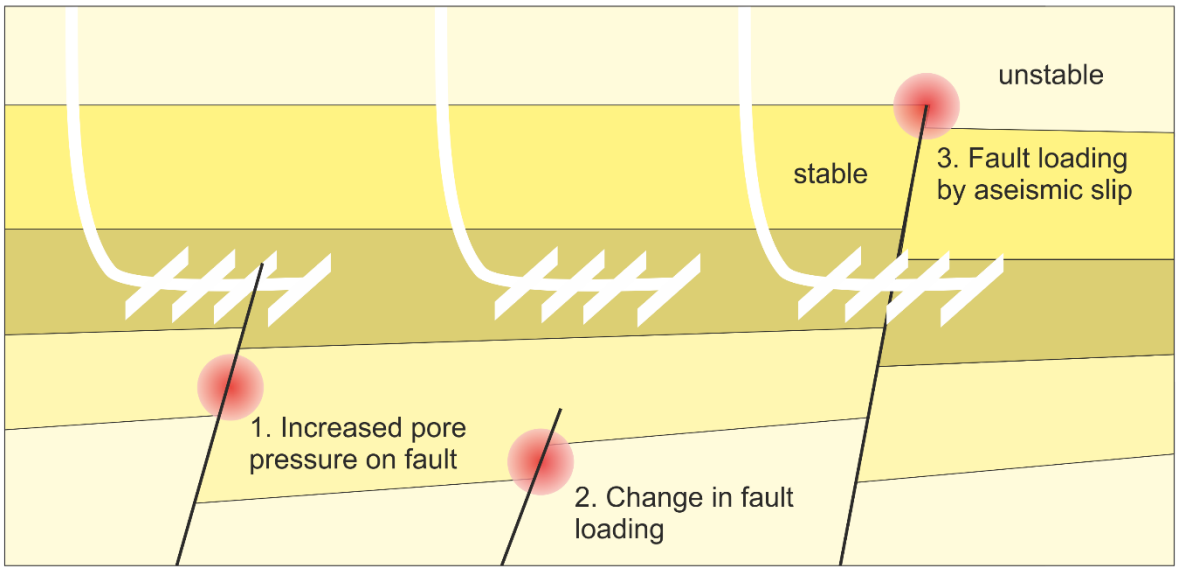

Figure 6. Conceptual diagram of HF earthquake triggering mechanisms. Three proposed mechanisms are displayed from left to right: direct pore pressure communication, poroelastic stress transmission, and pore pressure causing aseismic slip. Figure adapted from Eyre *et al*., (2019b).

5.1 PORE PRESSURE CHANGE

It is well documented that increased pore fluid pressures at depth resulting from fluid injection can trigger slip on pre-existing faults that are already close to failure, with examples caused by both waste-water disposal in deep disposal boreholes (Ellsworth, 2013; Rubenstein and Mahani, 2015) and hydraulic fracturing for shale gas production (Schultz *et al*., 2017; Yoon *et al*., 2017). The Coulomb failure criterion relates the shear stress acting parallel to the fault plane and the normal stress acting perpendicular to the fault plane and provides a criterion for frictional sliding of a pre-existing fault:

$$\tau = \mu_s \sigma_n \tag{1}$$

where τ is the shear stress, μ_s is the coefficient of internal friction and σ_n is the normal stress. Slip will occur if the ratio of shear stress to normal stress equals or exceeds the frictional sliding resistance. The presence of pore fluid modifies this to:

$$\tau = \mu_s (\sigma_n - P_f) \tag{2}$$

Where P_f is the pore fluid pressure. Increased fluid pressures decrease the effective normal stress, which holds faults locked, releasing previously accumulated strain energy (Healy *et al*., 1968; Raleigh *et al*., 1976). The critical conditions can be illustrated by considering the stress state of a fault of arbitrary orientation with respect to the far-field effective stress (Figure 7 (a)). Both the normal stress, σ_n and the shear stress, τ, acting across and along the fault are a result of the pre-existing state of stress on the fault. Increasing pore pressure reduces the effective normal stress, σ_n' , and slip is triggered when the shear stress τ, equals the frictional strength, $\mu_s (\sigma_n - P_f)$

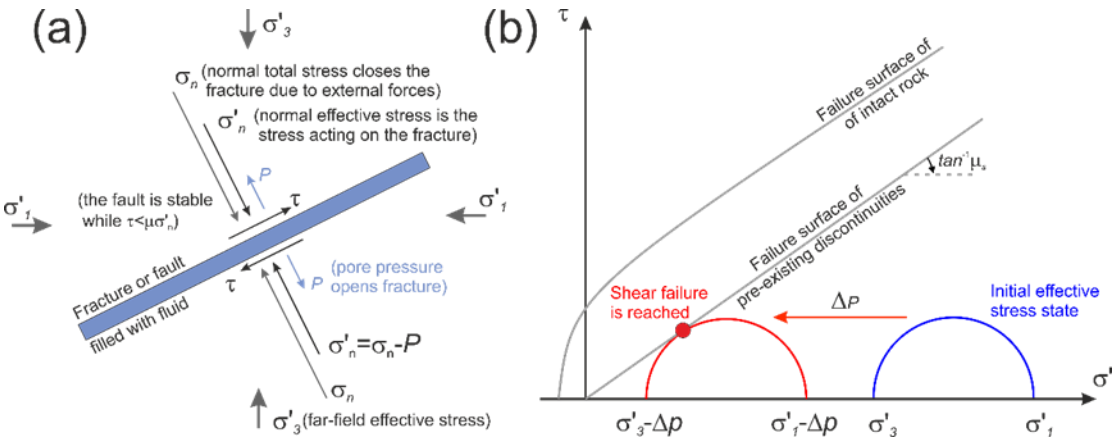

Figure 7. (a) Shearing of a jointed block (subjected to normal stress, σ_n , and a shear stress, τ, with fluid inside the joint at pressure P. Slip along the joint is triggered when the shear stress τ is equal to the frictional strength $\mu_s\left(\sigma_n - P_f\right)$. (b) Mohr circle diagram showing the effect of increased fluid pressure on a fault. Normal stress is on the horizontal axis and shear stress on the vertical axis. The Mohr circle shows the range of stresses acting on a plane at one location depending on orientation. The maximum and minimum normal stresses acting in any given location are σ_1 and σ_3. The failure envelope is shown by a black line whose slope is equal to the coefficient of static friction. When fluid pressure (P) is increased, normal stresses are reduced by P, resulting in new normal stresses σ_1' and σ_3', moving the Mohr circles to the left. This means that the Mohr circle intersects with the failure envelope allowing slip on suitably oriented faults.

5.2 POROELASTIC EFFECTS

The addition or removal of mass in the sub-surface can also compress or decompress fluids within pore spaces without any change in pore fluid content. This effect is known as the poroelastic response of the rock mass and also causes deformation and change in the stress state. The injection of fluid during hydraulic fracturing will result in such a poroelastic response, causing deformation in the surrounding rocks without any direct hydraulic connection to the stimulated region (e.g., Segall and Lu, 2015), potentially changing the stress on surrounding faults that may already be close to failure. It has been suggested that this mechanism may be an important factor in the activation of more distant faults in both waste-water disposal (e.g., Goebel *et al*., 2017) and hydraulic fracturing operations (e.g., Deng *et al*., 2016).

5.3 ASEISMIC SLIP

Where hydraulic fracture fluids intersect a fault, aseismic slip or creep may occur along the fault (e.g., Bhattacharya and Viesca, 2019). In this model, HF causes slow slip or creep on a frictionally stable part of a fault close to the stimulated volume that outpaces the pore pressure migration front. As aseismic slip accumulates, it progressively loads other parts of the fault system that are frictionally unstable, eventually resulting in rupture of these weaker segments of the fault. In this model direct hydraulic connection may be restricted in extent, only causing nearby aseismic slip that subsequently triggers more distant seismic slip (Eyre *et al*., 2019b). The aseismic fault slip model is supported by the observation that only a small proportion of the moment from the injection process is released by seismic events (Goodfellow *et al*., 2015), and by laboratory experiments that suggest that frictional resistance in fine-grained, clay or organic rich rocks increases with slip velocity in accordance with rate-state friction theory (Cappa *et al*., 2019).

6 Geological Susceptibility

The occurrence of HF induced seismicity in some areas and not others is often explained in terms of geological susceptibility. One of the most cited geological factors is the influence of

basement faults and there is considerable evidence that HF operations in deeper shale intervals, close to crystalline basement are more likely to induce larger earthquakes (Pawley *et al*., 2018; Skoumal *et al*., 2018a). In some cases, the target formations are within a few hundred meters of the basement and depths of induced earthquakes range from just above the target (Eyre *et al*., 2019a) to within the crystalline basement (Lei *et al*., 2017). This has led several authors (e.g., Anderson & Underhill, 2020; Corlett *et al*., 2018) to suggest that deeper operations increase the likelihood of interactions between HF and basement-rooted faults. In cases where earthquakes were located just above the target formation, there appears to be some correspondence to the sedimentary termination of basement-rooted faults (Eaton *et al*., 2018).

Similarly, research by Goebel *et al*., (2017) and Savage & Brodsky (2011) suggests that fault maturity may play an important role in the observed frequency-magnitude distribution of induced earthquakes, with older, more mature Precambrian faults that have smoother surfaces resulting in larger slip and an increase in the ratio of larger events to smaller ones than younger, less mature Palaeozoic faults with rougher surfaces.

High in-situ overpressure in shale formations, where the pore pressure is significantly above hydrostatic, has also been suggested as a controlling factor for earthquakes induced by HF. Eaton and Schultz (2018) show that earthquakes induced by HF in the Montney and Duvernay formations are strongly clustered within areas where the pore-pressure gradient exceeds 15 kPa m^{-1}, while they are absent elsewhere. Similarly, in the Bowland shale play the PNR-1z well was interpreted to be significantly over pressured with a pore pressure gradient of 15.61 KPa/m. As a result, target formation overpressure has been interpreted as a proxy for slip potential (Sibson, 2020).

If the orientation and magnitude of the principal stresses are known these can be used to estimate slip tendency (the ratio of shear stress to normal stress) for different fault orientations and pore pressures. This can be defined as

$$T_s = \mu_s \frac{\tau}{(\sigma_n - P_f)} \geq \mu_s \qquad (3)$$

For a given pore pressure, slip tendency is expected to be highest for those faults that are most favourably oriented. However, some studies (e.g., Shen *et al*., 2019) have suggested that many fault orientations would be unstable under reasonable HF stimulation pressures, thus relaxing the requirement for a fault to be optimally oriented. An example of this is shown in Figure 8, which shows stereographic plots of slip tendency calculated for different strikes and dips of fault in a strike slip stress regime ($S_H > S_V > S_h$) where the magnitudes of the principal stresses are S_H = 124 MPa, S_V = 84 MPa and S_h = 65 MPa, and the trend of S_H is 41° for three different pore fluid pressures. Slip tendency is greatest for steeply dipping strike slip faults with strikes that are either NNW-SSE or ESE-WNW. Left-lateral slip should occur along NNW-SSE faults and right lateral slip lateral slip should occur along ESE-WNW faults. As pore pressures increase, slip tendency also increases even for those faults that are not optimally oriented.

Finally, tectonic strain rates have also been suggested as a factor controlling the spatial distribution of HF-induced seismicity in Alberta and BC (e.g., Kao *et al*., 2018). However, in many areas of the central United States and Canada tectonic strain rates are very low (Calais *et al*., 2016; Ellsworth *et al*., 2015) and HF induced earthquakes dominate those of tectonic origin.

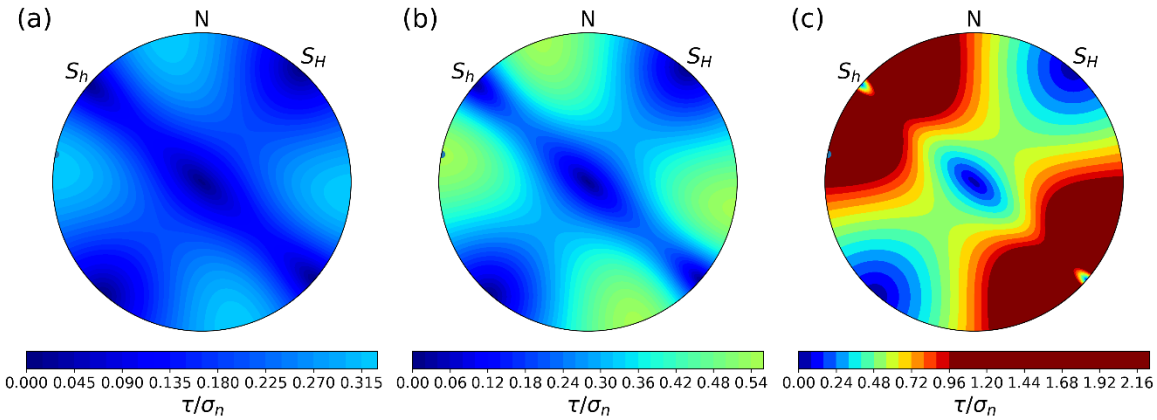

Figure 8. Stereographic plots showing slip tendency (ratio of shear to normal stress) for different fault orientations in an Andersonian stress field where the magnitudes of the principal stresses are S_H = 124 MPa, S_V = 84 MPa and S_h = 65 MPa, and the trend of S_H is 41° for pore fluid pressures of: (a) P = 0 MPa; (b) P = 33 MPa; and (c) P = 62 MPa.

7 Geology and Tectonics of Northern Ireland

Northern Ireland can be divided into four main geological regions distinguished by the age, type and setting of the rocks contained within them (Figure 9). Areas 1 and 2 are dominated by older metamorphic (1) and sedimentary (2) rock types, ranging in age from Mesoproterozoic to Lower Palaeozoic, together with major igneous intrusions. These rocks are not considered to contain any potential hydrocarbons resources. Areas 3 and 4 both contain younger sedimentary rocks some of which are considered to potentially contain significant hydrocarbons resources, including shale oil or gas.

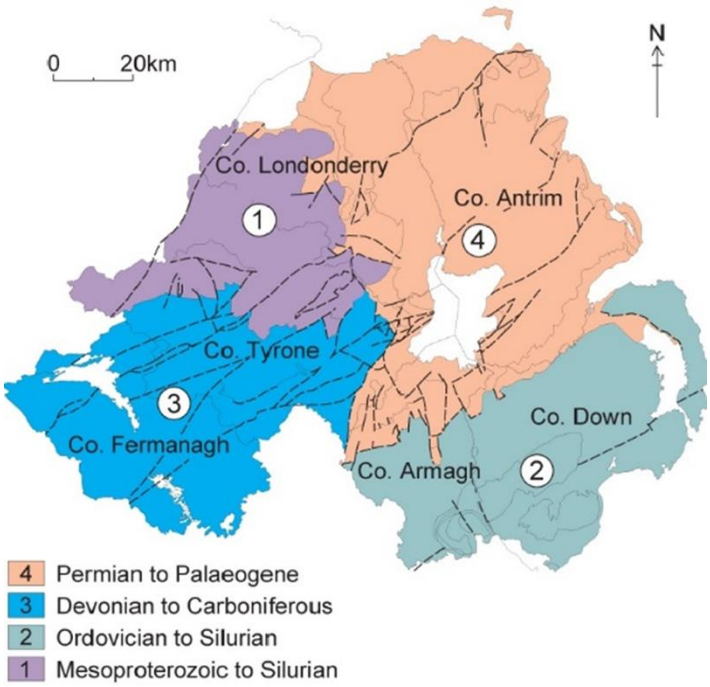

Figure 9. Major geological regions of Northern Ireland (From Mitchell, 2004). Dashed lines indicate some of the regionally important faults mapped at the surface.

7.1 LOUGH ALLEN BASIN (LAB)

In the southwest, Area 3 comprises Devonian and Carboniferous rocks and it is dominated by the Northwest Irish Carboniferous Basin which in Northern Ireland is sub-divided into the Omagh, Slieve Beagh and Lough Allen Basins (LAB), the last of which extends into the Irish Republic. The structure and geological history of the LAB has been described in several papers and reports (e.g. Philcox *et al*., 1992; Beach, 2006; CSA, 2006; Worthington & Walsh, 2011). Other studies have looked at tectonism in different geological periods across Northern Ireland (e.g., Anderson *et al*., 2018).

The LAB is bounded by major faults on its north-western (SW-NE trending Ox Mountains Fault), southern (WSW-ENE Curlew Mountains Fault) and northern (NW-SE Lower Lough Erne Fault) margins. Internally the basin is bisected by the SW-NE trending Belhavel – Castle Archdale Fault complex which extends to the northeast as the Omagh Thrust and southwest into County Mayo (Figure 10). These faults have a long geological history and mark the boundaries of different basement blocks that underlie the Lough Allen Basin and the areas adjacent to the basin. At the surface these major bounding and intrabasinal faults may not always be continuous (e.g., the Clogher Valley Fault in Kelly and Jones, 2020), but appear to be rooted in the basement.

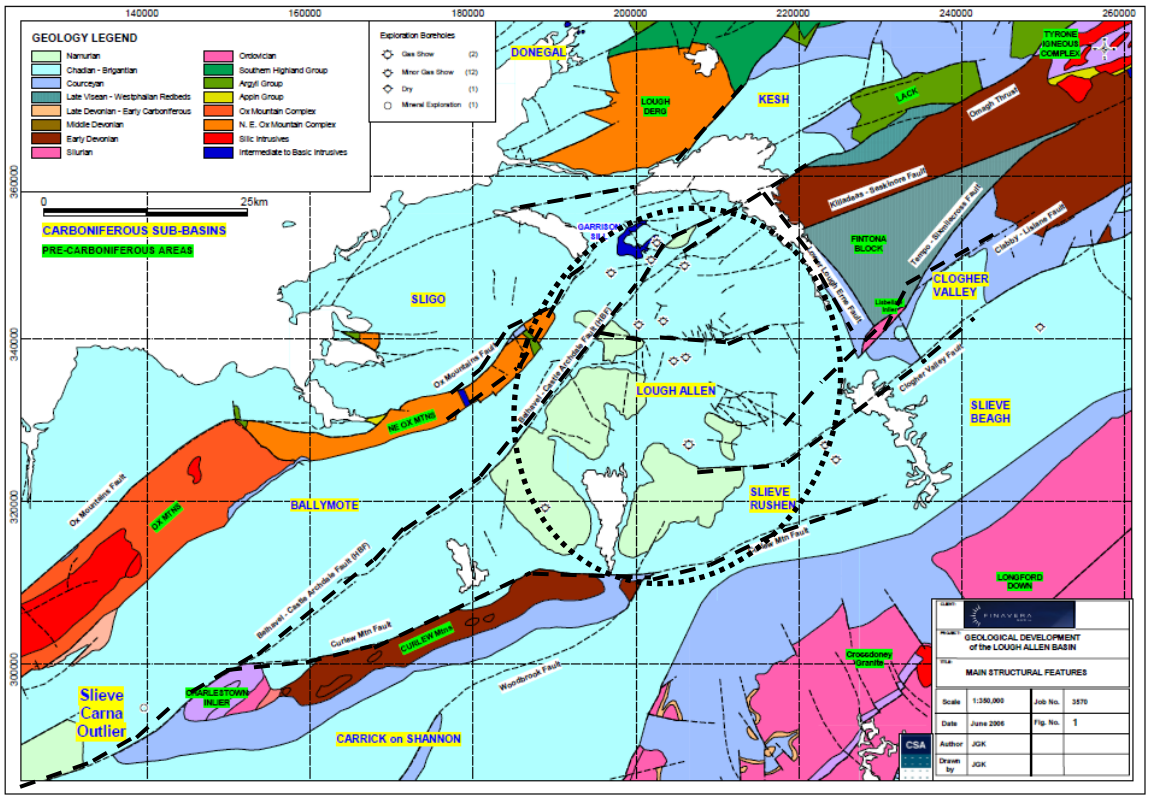

Figure 10. Tectonic setting of the Lough Allen Basin (from CSA, 2006). Dotted ellipse indicates main are of basin. Dashed lines indicate main basin bounding and intrabasinal fault zones.

The main targets for gas exploration in the LAB are the Lower Carboniferous Mullaghmore and Dowra Sandstones and the Bundoran Shale. The former are tight gas sandstones with low permeability. Eight wells have been drilled in the NI part of the LAB. In these, the top of the Bundoran Shale Formation ranges from 625 to 863 metres below surface and the base from 1085 to 1180 metres below surface, with thicknesses varying from 427 metres to 555 metres. Most wells show there is at least 800 metres of earlier Carboniferous sediments below the base of the Bundoran Shale Formation. A single well penetrates the pre-Carboniferous basement 810 metres below the Bundoran Shale.

In comparison to most sedimentary basins that have been explored for oil and gas, there is relatively little exploration data for the LAB. One regional 2D seismic survey has been shot

across the Lough Allen Basin in 1982, totalling 770 km. Data quality is variable. Faults with a range of trends can be identified from the data, however, it is often difficult to follow the faults to the surface as the reflector continuity breaks up within the fault zones. The top of the basement cannot be interpreted with any great confidence, but there is a variable thickness of sedimentary rocks between the target Bundoran Shale Formation and the basement. In some areas, this may be up to 3km thick and consist of early Carboniferous and Devonian rocks.

Additional geophysical surveys such as the Northern Ireland regional gravity survey, the Tellus airborne aeromagnetic, radiometric and electrical conductivity survey and local magnetotelluric (MT) surveys also provide some information about the nature of the geological structure and subsurface geology. Anderson et al. (2018) used Tellus data to show that there had been kilometre-scale sinistral displacement on NE-SW faults and dextral displacement on NNW-SSE faults across Cretaceous to Palaeogene aged basaltic dykes that trend in NNW-SSE, NW-SE and WNW-ESE directions, reflecting post-intrusion strike slip movement (Cooper et al., 2012)

There is relatively little information about the current stress regime in the Lough Allen Basin and whether or not faults are critically stressed. During flow tests in the Mullaghmore Sandstone it was observed that this formation was under-pressured by about 200 psi which would reduce the effective vertical stress component and favour strike slip movement should failure occur along existing faults. Borehole image logs run in several wells indicate the presence of open fractures in places and their orientation is consistent with a regional stress regime dominated by NW-SE compression similar to that found elsewhere in the UK (Baptie 2010).

7.2 THE RATHLIN BASIN

In area 4, the Rathlin Basin is one a number of Permo-Triassic sedimentary basins in Northern Ireland, the surrounding offshore areas and southern Scotland. These basins typically have a polyphase history, with earlier Carboniferous sedimentary rocks preserved beneath the main Permo-Triassic sedimentary fill. In the offshore areas to the east and in southern Scotland the basins have a N-S orientation having developed in response to E-W extension. In Northern Ireland, whilst this N-S orientation is evident in faults that have been active in the Permo-Triassic and later, the basins have also been largely controlled by pre-existing faults with a NE-SW Caledonian trend – in the Rathlin Basin this has been the Tow Valley Fault (Figure 11).

The bedrock geology at the surface of the Rathlin Basin is dominated by a thick cover of Palaeogene basalts of the Antrim Lava Group, overlain by a variable cover of superficial sediments. The basin takes the form of a half-graben, with Carboniferous to early Jurassic sedimentary rocks thickening towards the Tow Valley Fault. Geological mapping of the surface bedrock gives very little indication of the nature of the geological structure within the basin.

The Ballinlea No. 1 well is the only modern oil and gas exploration well in the basin and was drilled to test conventional Triassic Sherwood Sandstone, Permian Enler and Carboniferous sandstone reservoir targets. The Carboniferous sequence included gas-bearing coals, an oil-bearing sandstone and mature organic-rich shales. There is also possible oil and gas potential within the Carboniferous Coal Measures and the Craigfad and Murlough Shale Formations. The drilled sequence was found to be normally pressured.

There is little exploration geophysics data for the Rathlin Basin and data quality is poor and sub-basalt imaging is difficult. The existing 2D seismic data is not of sufficient quality to allow detailed interpretation to be carried out with any confidence. As a result, the detailed structure within the basin is poorly known. With the exception of the Tow Valley Fault, it is not known which other faults may be rooted in the basement. Gravity modelling has been used to produce structural models, but these do not have the resolution of good seismic data, and the models are non-unique with limited well control to calibrate them. The gravity models suggest that the Carboniferous unconventional reservoir targets may be of the order of 500 – 1000 metres above the basement.

High resolution Tellus airborne geophysics (magnetics, radiometrics and conductivity), airborne full tensor gravimetry and magnetotellurics (MT) surveys have all been used to help reveal the nature of the subsurface geological structure in the Rathlin Basin (Figure 11). The aeromagnetic anomaly data is dominated by the signal from the highly magnetic Antrim basalts and they

clearly pick out faults and other discontinuities that cut the basalt outcrop whereas the gravity data can be interpreted in terms of differences in rock densities and can provide information about sedimentary thicknesses and faults.

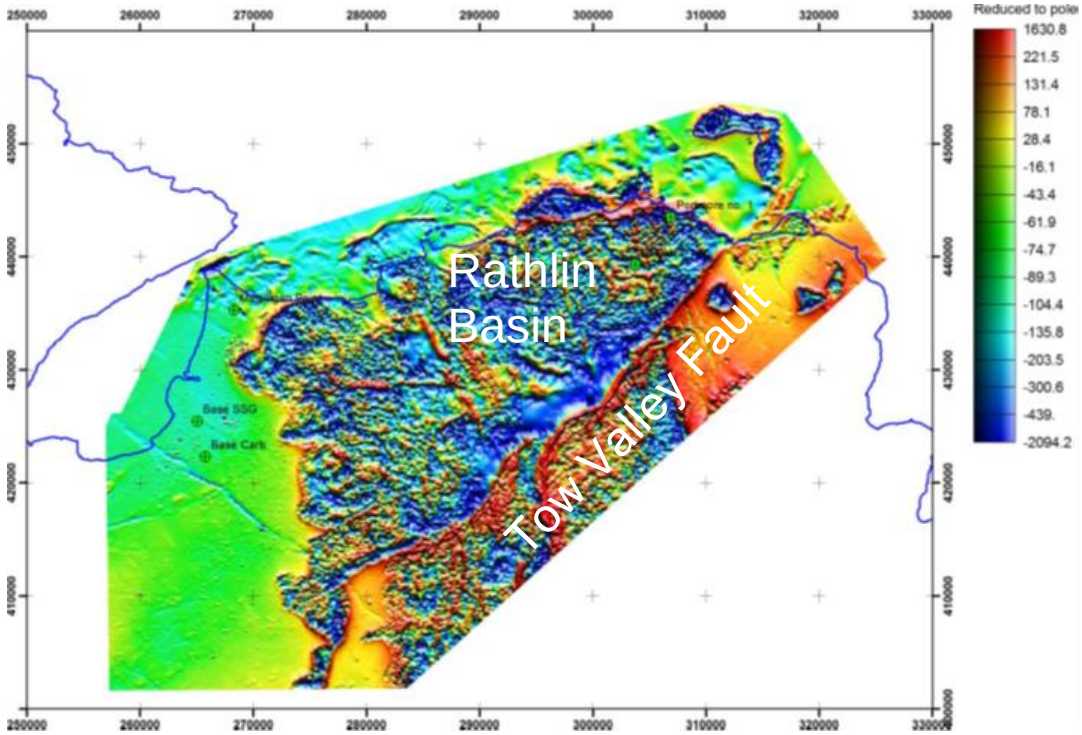

Figure 11. Reduced-to-pole aeromagnetic anomaly map, based on Tellus data. The Tow Valley Fault, forming the SE boundary to the Rathlin Basin, is clearly visible as the NE-SW trending linear anomaly. GSNI Tellus regional airborne geophysical survey data is published by OpenDataNI and licensed under OGL (Open Government Licence).

7.3 TECTONIC EARTHQUAKE ACTIVITY IN IRELAND

The historical seismicity of Ireland has been studied by a number of researchers including Davison (1924) and Richardson (1975) and a review of published data (Baptie *et al*., 2016) confirmed that earthquake activity is very low. Historical accounts reveal only 26 events in the period 1500 to 1970, which can be deemed credible. Half of these accounts can be attributed to earthquakes that occurred outside Ireland, in England, Scotland or Wales, where there is substantial evidence of widely felt and occasionally damaging earthquakes stretching back many hundreds of years. These were nearly all events of around magnitude 5 M_L or above that occurred in the western part of Britain and were widely felt across Britain and Ireland. The other thirteen events occurred in Ireland and the immediate offshore area. All of these have low intensities suggesting that these were small earthquakes. Nearly all the historical activity is concentrated around the coast and there is an almost complete absence of seismicity inland (Figure 12a).

Instrumental data from the Dublin Institute of Advanced Studies (DIAS) and the British Geological Survey (BGS) catalogues (Figure 12b).also confirm these low rates of seismic activity. Ireland had at least one operational seismograph throughout the 20th Century and the first seismograph network was installed in 1977. Almost all the instrumental seismicity lies in areas where historical earthquakes have occurred; mainly in Wicklow and the Irish Sea; Wexford, Waterford and Cork on the south coast of Ireland and, Donegal in the north. The exception to this is the magnitude 4.0 M_L earthquake off the coast of Mayo in 2012, which is the largest Irish event in the catalogue. Nearly all the seismic activity in Ireland, both instrumental and historical is concentrated around the coast and there is an almost complete absence of seismicity inland, with only two instrumentally recorded earthquakes in County Leitrim.

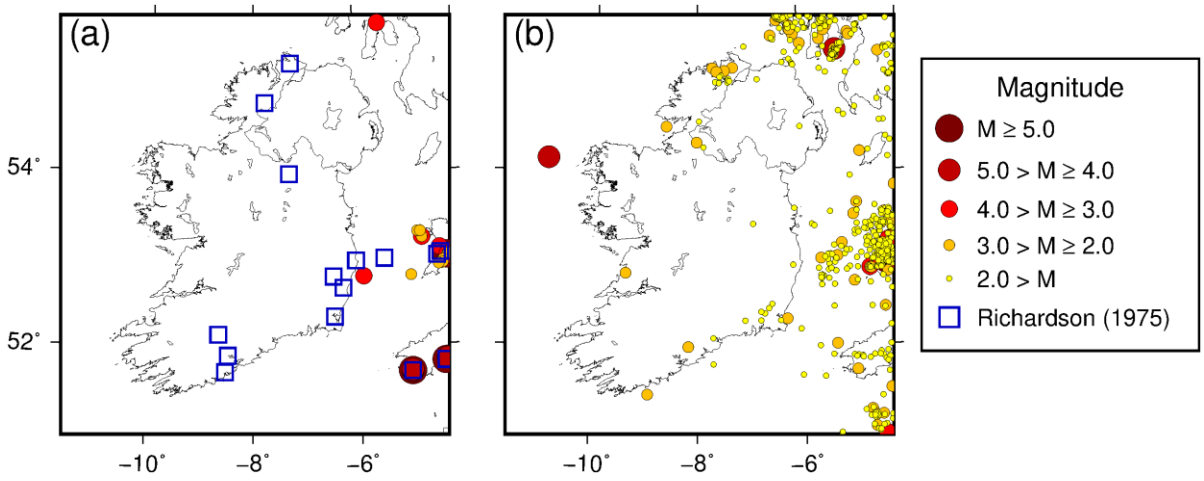

Figure 12. Historical (a) and instrumentally recorded (b) seismicity in and around Ireland from the DIAS and BGS catalogues. Symbol size is proportional to magnitude. Blue squares show historical earthquakes identified by Richardson (1975) that cannot be assigned a magnitude.

Baptie *et al*. (2016) used the combined historical and instrumental catalogue to determine an earthquake activity rate for Ireland, i.e. the number of earthquakes above a given magnitude in a given period of time. This suggests an earthquake with a magnitude of 4 Mw or greater approximately every 476 years. This contrasts with a rate for the UK of a magnitude 4 Mw earthquake every six years. However, the results strongly depended on assumptions of catalogue completeness, which highlights the problem of estimating reliable rates in low seismicity regions, where data are sparse.

8 Hazard and risk

Hazard for tectonic earthquakes can be considered a function of the frequency of earthquakes in space and earthquake size, and a model that describes the strength of the ground shaking at a particular location for a given earthquake. The former is often based on historical earthquake data. A similar approach can be used to assess the hazard from induced seismicity, however, for new HF operations there will be no data to develop such models. This requires the use of a proxy such as data from an analogous region and/or operational parameters that can be linked to earthquake activity. In addition, tectonic earthquake activity is usually assumed to be stationary, i.e., it does not change with time, whereas induced seismicity will have a strong dependence on both the locus and nature of operations. As a result, the hazard will be time dependent and increase with factors such as the number of wells.

Risk is the probability of loss or damage and is a function of both exposure and vulnerability, e.g., the number of buildings exposed to shaking and the susceptibility of those buildings to damage, as well as the hazard. Accordingly, risk may be very different in a densely populated area of the UK than in a remote region of North America even if the hazard were comparable.

8.1 DISTRIBUTION IN SPACE AND TIME

The relationship between the magnitude and number of tectonic earthquakes follows the well-known Gutenberg-Richter relationship (Gutenberg and Richter, 1954), where the number of earthquakes above a given magnitude decreases exponentially as magnitude increases,

$$\log_{10} N = a - bM \tag{4}$$

where, *N* is the number of earthquakes and *M* is magnitude. The constant *a* is a function of the total number of earthquakes in the sample and is known as the earthquake rate. This is

commonly normalised over a period of time, such as a year. More active regions have higher values of *a* which reflects the greater number of earthquakes. The constant *b* gives the proportion of large events to small ones and is commonly referred to as the *b*-value. In general, *b*-values are close to unity for tectonic earthquakes, so for each unit increase in magnitude, the number of earthquakes reduces tenfold. This relationship gives us a means to estimate the likelihood of larger earthquakes from an initial set of smaller events if the b-value is known (Weichert, 1980).

Induced earthquakes are also widely observed to follow the Gutenberg-Richter law (van der Elst *et al*., 2016), suggesting that the magnitudes of the induced events are controlled by similar processes to those of natural events. Atkinson *et al.* (2020) suggests that earthquakes associated with HF wells in western Canada between 2010-2018 follow the Gutenberg-Richter Law with approximately 60 events with magnitudes of 3.0 Mw or greater and seven events of 4.0 Mw or greater. Interestingly, *b*-values for induced microseismicity are often significantly higher than for tectonic seismicity. This is important because the *b*-value is used to estimate the likelihood of larger events and a high value reduces this.

Figure 13 shows the frequency magnitude distributions for induced seismicity recorded by downhole geophones during operation in the PNR-1z and PNR-2 wells, Preston New Road, Lancashire, together with the maximum likelihood estimates of the *b*-value and activity rate for calculated completeness magnitudes of -1.0 Mw. The *b*-values of 1.53 and 1.32 are robustly higher than those observed for tectonic seismicity.

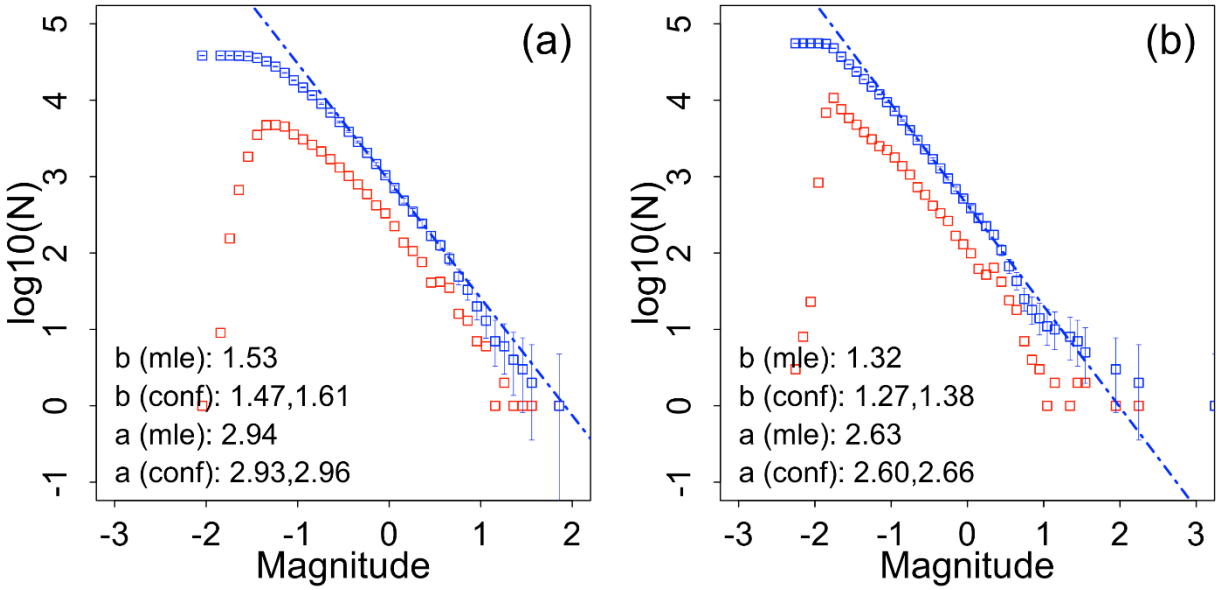

Figure 13. Frequency magnitude distributions for the PNR-1z (a) and PNR-2 (b) downhole catalogues. Red and blue squares show incremental and cumulative data. Error bars show 95% confidence limits determined from a χ2 distribution with the number of degrees of freedom specified by the cumulative number of events. The blue dashed lines show the maximum likelihood estimates of the b-value and activity rate for a completeness magnitude of -1.0 for the downhole catalogues and -0.5 for the surface catalogues. Confidence limits are from bootstrap resampling. From Baptie *et al.* (2020).

8.2 INJECTED VOLUME AND HAZARD

McGarr (2014) proposed that the maximum magnitude of earthquakes induced by fluid injection is limited by the injected volume and that the maximum seismic moment increases linearly with the injected volume at a rate equal to the shear modulus. However, other authors (e.g., Lee *et al*., 2019) have shown that this limit does not always hold and that maximum magnitudes are consistent with sampling from an unbounded Gutenberg-Richter distribution (Van der Elst *et al*., 2016). Shapiro *et al*., (2010) suggested that a seismogenic index, Σ, can be used to compare

the rate of induced seismicity in different environments. This relates the number of events above a given magnitude to the injection volume but is independent of injection parameters and depends only on tectonic features. Specifically, the number of earthquakes (N) above some threshold magnitude (M_c) is given by,

$$\log_{10} N(M \geq M_c) = \Sigma + \log_{10} V - bM_c \quad (5)$$

Where V is the volume injected and b is the b-value. Previous studies have shown that Σ values vary by ~10 orders of magnitude across a selection of sites, demonstrating clear variations in the susceptibility of a region to induced seismicity. This relationship is analogous to the Gutenberg-Richter relationship in equation (4). If the events occur independently, the Poisson distribution can be used to compute the occurrence probability of events with magnitude larger than a given magnitude in a specified time interval. For example, Figure 14 (a) shows the probability that at least one event with a magnitude of 2.5 or larger will occur as function of injected volume for different values of Σ. As Σ decreases, so does the probability of occurrence. Figure 14 (b) shows the probability of an event above a specific magnitude given the total volumes injected during HF operations in the PNR-1z and PNR-2 wells at Preston New Road, Lancashire.

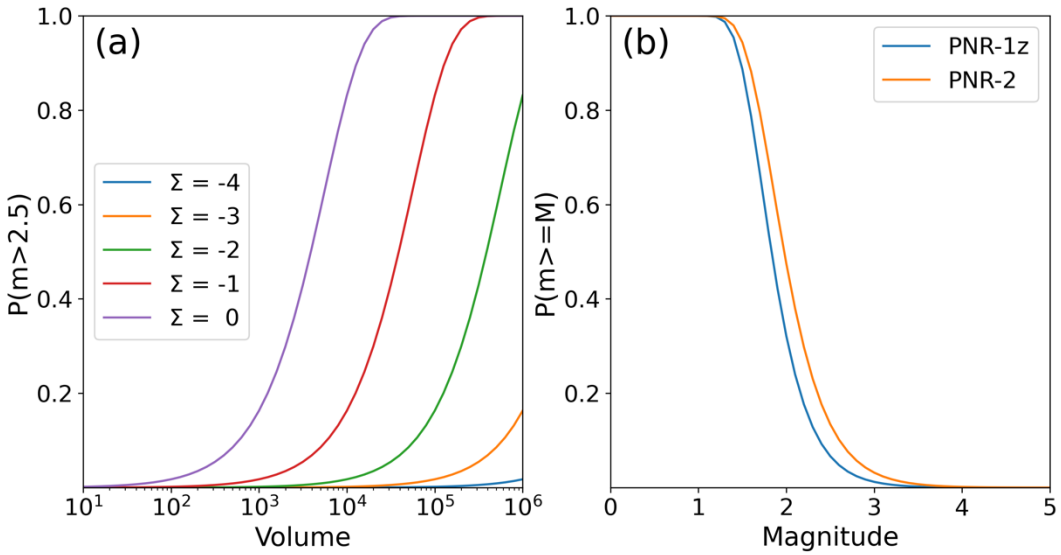

Figure 14. (a) Probability that events with M > 2.5 will occur as a function of injected volume for different seismogenic indices and a b-value of 1.5. (b) The probability of an event above a specific magnitude given the total volumes injected at PNR-1z and PNR-2 (3876 and 2564 m^3, respectively), b-values of 1.5 and 1.3 and a seismogenic index of -1.0.

Hallo *et al*., (2014) follow a similar approach to McGarr (2014) and relate cumulative seismic moment, M_0, release to injected volume, V,

$$\sum M_0 = SE\ \mu|\Delta V| \quad (6)$$

where the parameter SE describes the correlation between the cumulative moment release and the cumulative injection volume and is defined as the "Seismic Efficiency" (Hallo *et al*., 2014). μ is the shear modulus. Hallo *et al.* (2014) combine the SE parameter with the Gutenberg-Richter law to estimate the magnitude of the largest induced earthquake. Both Verdon and Budge (2018) and Clarke *et al*. (2019) applied this approach to estimate maximum magnitudes during HF operations.

Figure 15 (a) shows earthquakes (red dots) and cumulative injected volume of fluid (blue line) as a function of time during HF operations in the PNR-1z well near Blackpool, Lancashire. Seismicity is strongly clustered during periods of injection and there was a hiatus in operations between early November and early December. Figure 15 (b) shows the cumulative seismic moment, calculated from the moment magnitudes for individual events, as a function of cumulative injected volume. Clarke *et al*. (2019) interpret the observed change in gradient of the

relationship between injected volume and seismic moment as evidence of a change in seismic efficiency that occurred when operations intersected an existing fault. This changing constant of proportionality highlights the difficulty in attempting to assess any scaling relationship between cumulative moment and volume and incorrect estimates could lead to under- or overestimates of the numbers of earthquakes.

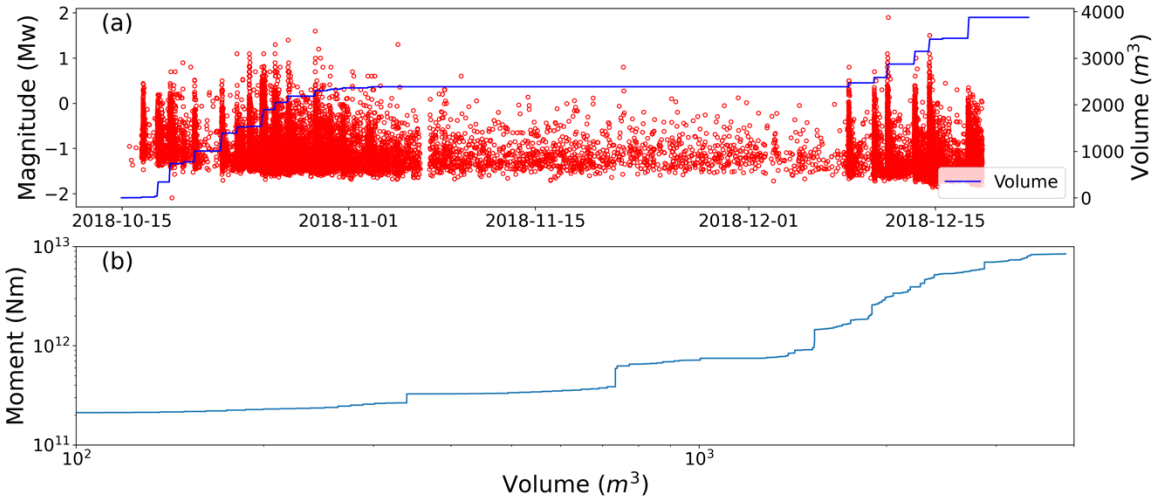

Figure 15. (a) Earthquakes (red dots) and cumulative injected volume of fluid (blue line) as a function of time during HF operations in the PNR-1z well near Blackpool, Lancashire. There was a hiatus in operations between early November and early December. (b) Cumulative seismic moment as a function of injected volume. Operational data from Preston New Road published by the Oil and Gas Authority [available at https://www.ogauthority.co.uk/exploration-production/onshore/onshore-reports-and-data/].

Statistical Epidemic Type Aftershock Sequence (ETAS) models typically used for forecasting clustered tectonic seismicity have also been applied to injection induced seismicity (Hainzl and Ogata, 2005). Conventional ETAS models describe seismicity as a result of two processes: spontaneous earthquakes generated by slow, steady, plate tectonic loading and earthquakes triggered by previous earthquakes. The spontaneous earthquakes are drawn randomly and independently from the Gutenberg-Richter law. Each spontaneous earthquake can trigger earthquakes according to the Omori law, which characterises the rate of decay of aftershocks as an inverse power law.

Bachmann *et al*. (2011) modelled the seismicity induced during a geothermal project in Basel, Switzerland, using an ETAS model with a background rate proportional to the flow rate at the well. Similarly, Lei *et al.* (2019) used an ETAS model to separate seismicity induced by HF in the South Sichuan Basin into events directly forced by fluid injection and Omori-type aftershocks. Mancini *et al.* (2020) modelled seismicity induced by HF operation at Preston New Road in 2018 and 2019 using a background seismicity rate that was also proportional to the injection rate.

Mancini *et al*. (2020) assessed the performance of different ETAS models by comparing the observed and modelled seismicity using log-likelihood scores to assess which models fitted the data best. Figure 16 shows cumulative log-likelihood scores as a function of time for each ETAS model considered by Mancini *et al*. (2020). The injection-rate driven ETAS2 models (ETAS2-bulk and ETAS2-specific) outperform other models. The out-of-sample ETAS2-unoptimized model scores better than all ETAS1 models and performs similarly to ETAS2-bulk during the first week of treatment of PNR-2. In other words, a model calibrated on PNR-1z data could have provided informative forecasts for PNR-2.

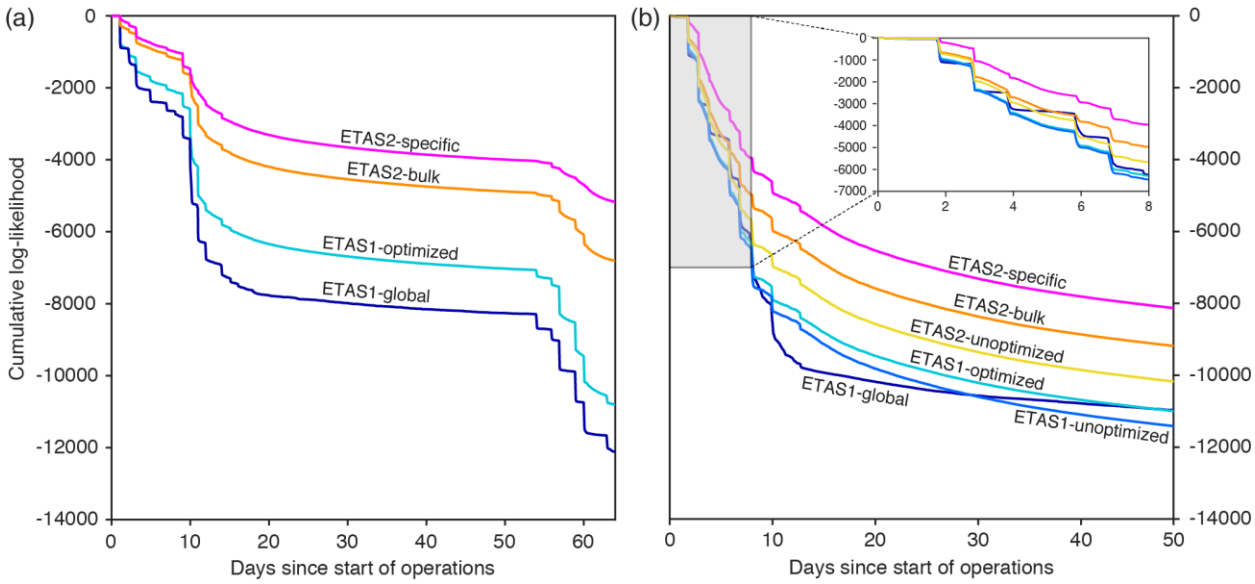

Figure 16. Cumulative log-likelihood timeseries. ETAS models tested on (a) PNR-1z and (b) PNR-2. From Mancini *et al*. (2020).

8.3 GROUND MOTIONS

The potential for damage from ground shaking depends on the nature and intensity of shaking, which in turn depends on the amount of seismic energy released by the earthquake, the distance from the earthquake source and the nature of the ground at a specific site. Empirical Ground Motion Prediction Equations (GMPEs) are commonly used to estimate possible levels of ground shaking that might result from future earthquakes (see Douglas and Aochi, 2008; Douglas and Edwards, 2016, for reviews). A GMPE predicts values of a particular ground-motion parameter, such as peak ground acceleration (PGA) or peak ground velocity (PGV), as a function of independent variables that characterise the radiation and propagation of seismic energy from the earthquake source to the site of interest. Earthquake Intensity, a qualitative measure of the strength of shaking of an earthquake determined from the observed effects on people, objects, and buildings (e.g., Grünthal, 1998) can also be used. The independent variables include the earthquake magnitude (or other measure of earthquake size), the distance from the earthquake source to the site, and the characteristics of the site itself.

Most GMPEs have been developed from observations of tectonic earthquakes for the purposes of earthquake resistant design where only larger earthquakes (e.g., M ≥ 4) are considered relevant. Relatively few GMPEs have been developed specifically for application to induced seismicity, where magnitudes may be smaller, and the events may be shallower. Douglas *et al*. (2013) derived a GMPE using ground motions from earthquakes induced at EGS in Europe and North America. Atkinson (2015) uses events with M 3–6 at distances less than 40 km that can be applied to small-to-moderate induced events at short hypocentral distances. Bommer *et al*. (2016) develop a ground-motion model specifically for induced seismicity in the Groningen gas field in the Netherlands. Cremen *et al*. (2019) modify the Douglas *et al*. (2013) model for application to induced seismicity at Preston New Road, Lancashire.

8.4 MAXIMUM MAGNITUDE

Maximum magnitude refers to the size of the largest possible earthquake in the region under investigation rather than the largest that has been observed. Early work suggested that the maximum magnitude for HF induced seismicity may be related to the size of the stimulated reservoir (e.g., Shapiro *et al*, 2010), the total injected volume (McGarr, 2014, Hallo *et al*., 2014) or the geomechanical properties of the reservoir rocks (de Pater and Baisch, 2011). However, it is generally acknowledged that such deterministic limits will not apply if earthquakes are triggered on existing faults that allow ruptures to propagate outside the stimulated reservoir (van der Elst *et al*., 2016). In this case, the maximum magnitude will be the maximum magnitude for

tectonic earthquakes, which is limited by possible fault rupture dimensions. However, defining a maximum magnitude is particularly challenging (Holschneider *et al*., 2011, 2014), particularly in intra-plate areas, where our understanding of the relationship between observed earthquake activity and faulting is often poor.

8.5 DAMAGE POTENTIAL

Following the magnitude 5.5 Mw earthquake in 2017 induced by operations at the geothermal site near Pohang, South Korea, Lee *et al*. (2019) concluded that a comprehensive risk-based approach that incorporates triggered large earthquakes is required to address the possible hazards from induced seismicity. However, there are relatively few published risk assessments for HF operations and even fewer quantify the risk in terms of damage or loss.

Edwards *et al*., (2020) present a pseudo-probabilistic seismic risk analysis applied to the largest of the induced events observed at Preston New Road, Lancashire. OpenQuake (Silva *et al*., 2014) was used to calculate the damage distribution for spatially variable ground-motion fields for different earthquake magnitudes calculated using a GMPE for induced seismicity (Atkinson, (2015). This incorporates both the exposure and fragility of different building types to different levels of ground shaking. The mean modelled occurrences of cosmetic and minor structural damage are consistent with reported damage. Edwards *et al*., (2021) conclude that significant occurrences of minor to major structural damage are likely for magnitudes in the range 3.5 to 4.5 M_L.

Cremen and Werner (2020) combine the Hallo *et al*. (2014) injection-volume-based statistical model of event magnitudes with a ground motion prediction equation (Cremen *et al*., 2019), and an exposure model, to quantitatively link the volume of fluid injected with the potential for nuisance felt ground motions during HF operations at Preston New Road, Lancashire. Their results suggest that ground motions equivalent in amplitude to that at which pile driving becomes perceptible may be exceeded in the location of at least one building for event magnitudes equal to or exceeding the current UK induced seismicity traffic light system “red light” event of 0.5 M_L, or injection volumes ≥ 1000 m^3. Cosmetic damage may occur in at least one building for Mw ≥ 2.1 or injection volumes ≥ 40,000 m^3. Cremen *et al*., (2020) suggest that this framework facilitates control of the injection volume ahead of time for risk mitigation and can be used to inform policy related to hydraulic-fracture induced seismicity.

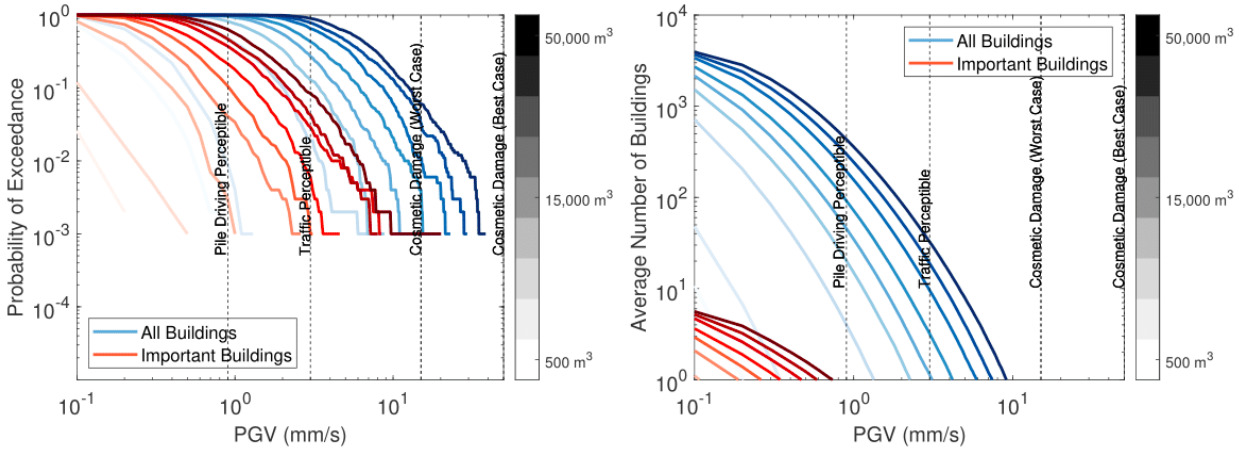

Figure 17. (Left) the probability of exceeding various PGV levels for at least one building (blue curves) and one important building (red curves) for specific injection volumes of 500, 1000, 5,000, 10,000, 15,000, 20,000, 30,000, 40,000 and 50,000 m^3. (Right) the average number of buildings (blue curves) and important buildings (red curves) at which various PGV levels are exceeded for volumes of 500, 1,000, 5,000, 10,000, 15,000, 20,000, 30,000, 40,000 and 50,000m^3). After Cremen and Werner (2020).

Figure 17 shows the probability of exceeding four different PGV levels for at least one building along with the average number of buildings at which various PGV levels are exceeded for

different injection volumes. Volumes of 5,000, 10,000, 15,000, 20,000, and 30,000 m^3 have approximately a 2%, 10%, 30%, 50%, and 80% chance, respectively, of generating ground motions that exceed the level at which traffic-induced vibration becomes perceptible at the location of at least one building in the exposure model. Cremen and Werner (2020) note that the largest contributor to exceeding either threshold is not always the maximum magnitude experienced, particularly for larger volumes of injected fluid, and that intermediate magnitudes are the main contributor to hazard and risk because they occur more frequently than larger magnitudes, however, the scenarios exclude the possibility of larger triggered earthquakes.

9 Mitigation

Following the felt seismicity induced by operations at Preese Hall in 2011 (Clarke *et al*, 2014), The UK Department for Energy and Climate Change (DECC, 2013) published a regulatory roadmap that outlines regulations for onshore oil and gas (shale gas) exploration in the UK. These regulations contain specific measures for the mitigation of induced seismicity including: avoiding faults during hydraulic fracturing; assessing baseline levels of earthquake activity; monitoring seismic activity during and after fracturing; and, using a 'traffic light' system that controls whether injection can proceed or not, based on that seismic activity.

Identification of faults in the locus of operations is challenging, even where 3-D reflection seismic data are available. The faults themselves may be of limited size and below the resolution of even detailed 3D surveys. They may also have small vertical throws, which makes them difficult to identify using surface acquisition. Additionally, basins such as the Bowland Shale have been subject to multiple episodes of deformation, resulting in structural complexity that makes data difficult to interpret (Anderson and Underhill, 2020). Even where faults can be identified it is difficult to tell if they might be seismogenic (Eaton *et al*., 2018).

Traffic light systems (e.g., Baisch *et al*, 2019) are one of the most widely implemented means of mitigating the risk of induced seismicity during HF operations themselves. These were originally developed for use in enhanced geothermal systems activity (e.g., Bommer *et al*., 2006; Majer *et al*., 2012) and are essentially control systems for management of induced seismicity that allow for low levels of seismicity but are intended to reduce the probability of larger events that may result in a concern for public health and safety by limiting/stopping operations at certain thresholds. These thresholds are generally based on levels of ground motion which may represent a hazard or a public nuisance. Table 2 shows the traffic light system used for a geothermal project in Basel, Switzerland and adapted from Bommer *et al*. (2006). This has four levels: green, where injection proceeds as planned; yellow/orange, injection proceeds with caution, possibly at a reduced rate; and, red, injection is suspended immediately.

While traffic light systems have been implemented in a number of basins, including British Columbia (British Columbia Oil and Gas Commission, 2012), the UK (Department for Energy and Climate Change, 2013), Alberta (Alberta Energy Regulator, 2015), California, (Code of Regulations section 1785.1 (2015)), and Ohio, (Administrative Code 1501:9-3-06), the limits for the cessation and recommencement of operations often differ widely. For example, in the UK, the magnitude limit of 0.5 M_L for the cessation of operations is considerably less than the limits in California (2.7 M_L), Ohio (2.5 M_L), or Alberta and British Columbia (4.0 M_L). Similarly, the red-light threshold in the United Kingdom only requires a temporary suspension of operations, whereas an exception in Alberta or BC requires complete cessation of operations at the well pad.

Traffic Light	Earthquake Activity	Earthquake Magnitude	Ground Velocity	Action
Green	None	$M_L < 2.3$	< 0.5 mm/s	Regular operation. Continue pumping.
Yellow	Some	$M_L \geq 2.3$	≤ 2.0 mm/s	Continue pumping but do not increase flow rate

Orange	Many	$M_L \leq 2.9$	≤ 5.0 mm/s	Maintain borehole head pressure below stimulation pressure
Red	Widely Felt	$M_L > 2.9$	> 5 mm/s	Stop pumping. Bleed off to minimum borehole head pressure

Table 2. Seismic response procedure used in Basel, Switzerland (and adapted from the traffic light system proposed by Bommer *et al*. (2006). The system is based on three independent parameters: (1) public response; (2) local magnitude (M_L); and, peak ground velocity (PGV)).

Also, despite their widespread implementation, traffic light systems have often failed to preclude larger earthquakes. For example, in the case of Basel, 2006 (Giardini, 2009), operations were stopped when the traffic light threshold of 2.9 M_L was exceeded, but this was still followed by even larger magnitude events that were strongly felt and resulted in superficial damage. The project was suspended and ultimately abandoned almost three years later following further study and risk evaluation after these seismic events (Giardini, 2009). In the UK eight events greater than the red-light threshold of 0.5 M_L occurred during operations in the PNR-1z well (Clarke *et al*, 2019). The last and largest, with a magnitude of 1.6 M_L, was felt locally. Similarly, the last HF stage to be stimulated during operations in the PNR-2 well was on 23 August 2019. However, events with magnitudes of 2.1 M_L and 2.9 M_L occurred approximately 40 hours and 72 hours after the last HF stage. The latter is the largest HF-related earthquake recorded in the United Kingdom to date, and it was strongly felt at distances of up to a few kilometres from the epicentre with maximum intensities of 6 EMS. This led to a premature end to operations in the PNR-2 well with only 7 (out of 47 HF) stages completed. The U.K. government subsequently announced an immediate moratorium on HF, due to the possibility of unacceptable impacts on local communities.

These shortcomings have led to suggested modifications to TLS to improve performance. Mignan *et al*. (2017) propose a data driven, adaptive traffic light system (ATLS) based on a statistical forecasting system to provide a risk-based safety target model of induced seismicity. Kwiatek *et al*. (2019) use near–real-time information on induced-earthquake rates, locations, magnitudes, and evolution of seismic and hydraulic energy by reducing well-head pressures or flow rates to control injection-induced seismicity.

Verdon and Budge (2018) and Clark *et al.* (2019) use a statistical model in which the rate of induced seismicity scales with the injection volume to retrospectively forecast expected event magnitudes during HF operations from the Horn River Shale, Canada and Preston New Road (PNR-1z), UK. The approach was also used in real time at Preston New Road to make operational decisions, however, it had to be retrospectively altered to account for changes in seismicity when operations intersected a previously unidentified fracture zone. Additionally, it did not perform well during operation in the PNR-2 well.

Finally, both Bachman *et al.* (2011) and Mancini *et al.* (2020) suggest that injection-rate driven ETAS models can contribute to useful probabilistic forecasts in future EGS experiments and shale gas developments, respectively.

10 Conclusions

Over the last decade the number of observations of induced earthquakes caused by HF operations around the world has increased as the shale gas industry has developed. Data from different basins in the US and Canada suggest that on average around 1% of HF wells can be linked to larger earthquakes (M>3). However, research has shown that in some areas of the US and Canada the percentage of wells associated with induced earthquakes is much higher (>30%). This variability is observed despite similar amounts of HF activity and is often explained

in terms of geological susceptibility. Proximity to critically stressed faults, fault maturity, high overpressures and tectonic strain have all been cited as causes for seismicity induced by HF operations. In a small number of cases HF operations have triggered earthquakes large enough to cause potentially damaging ground motions. Such earthquakes cannot be confidently predicted in advance of operations. These observations suggest that the risk from induced seismicity during HF operations is not negligible.

Earthquakes with magnitudes greater than around 2 result from slip on existing faults that is triggered by stress perturbations caused by the injection of fluid during the HF process. The size of the earthquake will depend on both the area of the ruptured part of the fault and the amount of slip. Since such faults may extend outside the stimulated zone, the maximum magnitude will be controlled by local geology and tectonics, not by operational parameters such as the total amount of fluid injected. As a result, the maximum magnitude is highly uncertain.

Induced earthquakes have been observed in a wide variety of geological settings and in areas where there are relatively few tectonic earthquakes. In some areas, the resulting hazard from induced earthquakes due to HF operations is significantly greater than the hazard from tectonic earthquakes. As a result, the low hazard from tectonic earthquakes in Ireland does not guarantee that the hazard from induced seismicity will also be low.

Induced earthquakes are likely to be clustered in space and time around the locus of HF operations. Hazard is likely to increase with the number of wells and will be highest during or shortly after HF operations. Hazard may also be a function of total injected volume, with larger injected volumes leading to more earthquakes and increasing the probability of larger events. However, the relationship between injected volume and earthquake numbers is largely empirical and still not fully understood. The potential for actual damage depends on the intensity of motion and both the number and vulnerability of buildings exposed to ground shaking. As a result, the risk of damage to buildings will be higher in densely populated urban areas than in rural areas. Risk studies for the UK have shown that cosmetic and minor structural damage may occur for earthquakes with magnitudes as low as 3.

There has been only a limited amount of oil and gas exploration in Northern Ireland. Consequently, the subsurface geology of the sedimentary basins with hydrocarbon potential is known only on a broad scale, or in detail at only a few well locations. Higher resolution geophysical data is needed to image detailed structure within the basin, identify faults and depth to basement in order to mitigate risk of induced seismicity from hydraulic fracturing of unconventional reservoirs.

The present-day stress regime and stress state of faults in the both the Lough Allen and Rathlin basins is poorly known. Well data suggest that Carboniferous sedimentary rocks in the Lough Allen Basin may be slightly under-pressured whereas data from the Rathlin Basin suggest a normal pressure gradient. Borehole imaging logs and breakout data from wells in Northern Ireland are consistent with the regional stress regime found elsewhere in the UK.

Current risk-mitigation strategies, such as avoiding faults, or the use of traffic light systems based on specific earthquake magnitude thresholds have often failed. There may be insufficient data to identify geological faults prior to operations and even where high resolution data are available, there may still be hidden faults. Similarly, the interaction of operations with existing faults may change earthquake activity rates, making larger earthquakes more likely. Statistical methods that relate operational parameters such as the volume of injected fluid or the injection rate to seismicity rates may allow useful probabilistic forecasts in the future but are likely to have considerable uncertainty without calibration for local conditions.

Glossary

b-value – A metric used to measure the relative proportion of small to large earthquakes.

Completion - the series of processes after drilling to bring a well into production. HF is a part of completion in many shale oil or gas wells.

Critically stressed – A description of the state of stress on a fault, where it is nearly ready to produce earthquake slip. To be critically stressed, a fault has to have the proper orientation in the present-day stress field.

Earthquake - The sudden shaking of the surface of the Earth caused by the passage of intense vibrations, or seismic waves, through the Earth. The seismic waves are generated by the sudden release of energy that results from the movement of adjacent rocks relative to each other. This movement takes place on pre-existing zones of weakness within the crust called faults and is generally a response to long term deformation and build-up of stress, caused by geological processes such as plate tectonics. When this stress exceeds the friction that resists the motion of the rocks on either side of the fault, they slide or slip past each other.

Earthquake hazard - Any property of an earthquake that might cause damage and loss. This may include ground shaking caused by seismic waves, relative displacement of a structure due to physical movement along the fault plane, or secondary hazards such as liquefaction.

Earthquake risk - The probability of loss or damage from earthquake activity. This may be quantified in terms of number of casualties, monetary loss, or repair costs.

Enhanced Geothermal System – A system process designed to extract heat energy from the subsurface. Wells are drilled and HF stages stimulation is used to enhance the permeability of hot and deep rocks. Due to the use of HF in this process, enhanced geothermal systems often encounter induced earthquakes similar to petroleum development HF cases.

Epicentre – The location of the point of initiation of an earthquake, projected to the Earth's surface.

Fractures – A planar discontinuity in a medium. Fractures that lack shear offset are called joints. Fractures can accommodate fluid-flow along the spaces between the rocks. In the context of HF-induced seismicity, these are intentionally stimulated by injection of fluid for resource production.

Fault – Discontinuities in a volume of rock where there has been displacement caused by relative movement of the rock-mass. Often simplified planar geometries are used to approximate the fault, although individual faults may in fact be much more complex. Faults are classified using the angle of the fault with respect to the surface (known as the dip) and the direction of slip along the fault.

Flowback – The process of flowing stimulation fluids back to the surface after HF completion.

Horizontal Well – A well that is drilled vertically, until reaching the target formation where it is deviated into a horizontal orientation. The section where the transition from vertical to horizontal occurs is called the "heel" and the end of the horizontal portion is called the "toe" (Figure 1). Typically, horizontal sections are up to 2 km in length.

Hydraulic Fracturing (HF) – A technique in which fluid is pumped into the ground at pressures higher than the smallest principal stress. Doing so causes fractures to slip, open, and propagate. These stimulated fractures enhance the permeability of the target formation. See King (2010) for a history of HF completion technologies, from a petroleum operator's perspective.

Hypocentre (also known as the focus) – The location (in the subsurface) where an earthquake initiates rupture.

Induced Seismicity – A type of earthquake activity that is caused or accelerated by human activities. Sometimes these earthquakes are distinguished into either triggered or induced,

depending on the degree of human influence. In this paper we make no distinction and refer to both types as induced.

Intensity - A qualitative measure of the strength of shaking of an earthquake determined from the observed effects on people, objects and buildings. Scales such as the European Macroseismic Intensity Scale (Grünthal, 1998) can also be used to describe possible impacts on different building types.

Local Magnitude (M_L) - The original earthquake magnitude scale developed by Richter (1935) based on observations of earthquakes in Southern California. Although the scale is only strictly applicable there, it has been used all around the world.

Magnitude - A measure of the amount of energy released during an earthquake. Magnitude is usually estimated from measured records of ground motion with specific corrections for distance. Most magnitude scales are logarithmic so that each whole number increase in magnitude represents a tenfold increase in measured amplitude and about 32 times the energy released.

Microseismicity – Stimulation of fractures during HF causes earthquake-like shear/tensile slip called microseismicity. Some authors ascribe this term to events below a specific magnitude level [Eaton, 2018b].

Mitigation – Procedures enacted by the HF operator to reduce the likelihood and severity of induced seismicity.

Moment (M_0) – A measure of earthquake size that depends on both the area of the rupture and the displacement on the rupture as well as the shear strength of the Earth. The larger the rupture area and the larger the displacement, the larger the moment. Seismic moment is usually estimated directly from recordings of earthquake ground motions.

Moment magnitude (M_w) – A measure of earthquake size based on seismic moment. It is generally considered to be the most reliable magnitude measure.

Pad – A surface location where horizontal well(s) are drilled by an operator. Pads may have a single well or multiple wells, sometimes as many as ten at a single location (Figure 1).

Permeability – The capacity for rocks to allow or resist fluid flow. A measure of the ease with which a fluid can pass through a porous medium.

Play – A term used to denote the extent of a target formation (or a package of formations) exploited by HF.

Porosity – The proportion of filled space to empty space in a rock.

Operator – The company who owns the HF pad and is responsible for completion.

Regulator – The institution responsible for the oversight of responsible operator development.

Rupture - The part of the fault that moves during an earthquake. This may only comprise a small part of the fault on which it occurs. The amount of displacement along the rupture is called the slip. The largest earthquakes occur on ruptures that are many hundreds of kilometres long, with areas of several thousand square kilometres, and that have displacements of many metres.

Secondary (or Enhanced) Recovery –A hydrocarbon recovery technique that uses the injection of fluids (e.g., water or CO_2) into a formation, with the intent to maintain or enhance reservoir pressure.

Shale – A term often used loosely in association with HF, sometimes as a synonym for play. Technically, shales are fine-grained sedimentary rocks deposited in laminations; often, they are highly impermeable. Shales may contain organic matter which matured into petroleum, and are thus a primary target for HF.

Stage – HF wells are completed in multiple stages, with up to many tens of stages per well (Figure 1). Stages are an isolated potion of the well, where HF stimulation occurs. Multiple stages along a well are completed sequentially.

Stimulation – A term used to describe fluid pumping to enhance permeability via HF. Stimulated fractures enhance the permeability of a target formation.

Traffic Light System – A regulatory framework intended to reduce the hazards and risks of induced seismicity. Often magnitude values are chosen at green, yellow, and red thresholds, respectively marking points to proceed, mitigate, and stop.

Data and Resources

Earthquake data for the UK is from the British Geological Survey UK Earthquake Catalogue © NERC 2020. Licensed under OGL (Open Government Licence) and available at http://earthquakes.bgs.ac.uk

Earthquake data for Ireland is published by Dublin Institute of Advanced Studies and is available at https://www.insn.ie/confirmed/.

Earthquake data for Canada from the Canadian Composite Seismicity Catalogue and available at https:// www.inducedseismicity.ca.

Earthquake data for the US is from the ANSS Comprehensive Earthquake Catalog (ComCat), credit: U.S. Geological Survey. Available at http://earthquake.usgs.gov/earthquakes/search/.

Well data for Alberta obtained from the Alberta Energy Regulator and available at https://www.aer.ca/data-and-publications.

Well data for British Columbia obtained from the B.C. Oil and Gas Commission and available at http://data.bcogc.opendata.arcgis.com.

Microseismicity and pumping data from operations at Preston New Road are obtained from the Oil and Gas Authority and available at https://www.ogauthority.co.uk/exploration-production/onshore/onshore-reports-and-data/.

GSNI Tellus regional airborne geophysical survey data is published by OpenDataNI and licensed under OGL (Open Government Licence). Available at https://data.gov.uk/dataset/88d90c6f-07ff-43ea-a594-d5a10602d175/gsni-tellus-regional-airborne-geophysical-survey-magnetics.

References

British Geological Survey holds most of the references listed below, and copies may be obtained via the library service subject to copyright legislation (contact libuser@bgs.ac.uk for details). The library catalogue is available at: https://envirolib.apps.nerc.ac.uk/olibcgi.

Anderson, E.M. (1905). The dynamics of faulting. *Transactions of Edinburgh Geological Society*, 8, 387–402.

Anderson, H., Walsh, J.J. and Cooper, M.R. (2018). The development of a regional-scale intraplate strike-slip fault system: Alpine deformation in the north of Ireland. *Journal of Structural Geology*, 116, 47-63. https://doi.org/10.1016/j.jsg.2018.07.002.

Anderson, I. & Underhill, J.R. (2020). Structural constraints on Lower Carboniferous shale gas exploration in the Craven Basin, NW England. *Petroleum Geoscience*, **26**, 303-324. https://doi.org/10.1144/petgeo2019-125

Atkinson, G.M. (2015). Ground-motion prediction equation for small-to-moderate events at short hypocentral distances, with applications to induced-seismicity hazard. *Bulletin of the Seismological Society of America*, 105(2A), 981-992.

Atkinson, G.M., Assatourians, K., Cheadle, B. & Greig, W. (2015). Ground motions from three recent earthquakes in western Alberta and northeastern British Columbia and their implications for induced-seismicity hazard in eastern regions. *Seismological Research Letters*, 86(3), 1-10

Atkinson, G.M., Eaton, D.W., Ghofrani, H., Walker, D., Cheadle, B., Schultz, R., Shcherbakov, R., Tiampo, K., Gu, J., Harrington, R.M., Liu, Y., van der Baan, M. & Kao, H., (2016). Hydraulic Fracturing and Seismicity in the Western Canada Sedimentary Basin. *Seismological Research Letters*, 87(3), 631-647. https://doi.org/10.1785/0220150263

Atkinson, G. M., Eaton, D. W., & Igonin, N. (2020). Developments in understanding seismicity triggered by hydraulic fracturing. *Nature Reviews Earth & Environment*, ***1***(5), 264–277. https://doi.org/10.1038/s43017-020-0049-7.

Babaie Mahani, A., Schultz, R., Kao H., Walker, D., Johnson, J. & Salas, C. (2017). Fluid injection and seismic activity in the northern Montney Play, British Columbia, Canada, with special reference to the 17 August 2015 Mw 4.6 induced earthquake. *Bulletin of the Seismological Society of America*, **107**(2), 542–552.

Babaie Mahani, A., Kao, H., Atkinson, G. M., Assatourians, K., Addo, K., & Liu, Y. (2019). Ground motion characteristics of the 30 November 2018 injection-induced earthquake sequence in northeast British Columbia, Canada. *Seismological Research Letters*, **90**(4), 1457–1467. https://doi.org/10.1785/0220190127

Bachmann, C., Wiemer, S., Woessner, J., & Hainzl, S. (2011). Statistical analysis of the induced Basel 2006 earthquake sequence: introducing a probability-based monitoring approach for Enhanced Geothermal Systems. *Geophysical Journal International*, 186, 793-807.

Baisch, S., Koch, C., & Muntendam-Bos, A. (2019). Traffic light systems: To what extent can induced seismicity be controlled? *Seismological Research Letters*, 90(3), 1145–1154. https://doi.org/10.1785/0220180337.

Bao, X., & Eaton, D. W. (2016). Fault activation by hydraulic fracturing in western Canada. Science, 354, 1406–1409. https://doi.org/10.1126/science.aag2583.

Baptie, B. (2010). Seismogenesis and state of stress in the UK. *Tectonophysics*, 482 (1-4). 150-159. https://doi.org/10.1016/j.tecto.2009.10.006.

Baptie, B., Jordan, C., Mosca, I., Cigna, F., Burke, S., McCloskey, J., Nic Bhloscaidh, M., Bean, C. & Möllhoff, M. (2016). *Final Report 2: Baseline Characterisation of Seismicity*. Joint Research Programme on the Environmental Impacts of Unconventional Gas Exploration and Extraction, Environmental Protection Agency, Ireland. ISBN: 978-1-84095-688-7. [Available at https://www.epa.ie/pubs/reports/research/ugeejointresearchprogramme/].

Baptie B., Segou M., Ellen R. & Monaghan, A. (2016). *Unconventional Oil and Gas Development: Understanding and Monitoring Induced Seismic Activity*. British Geological Survey Open Report, OR/16/042. 92pp. [Available at https://www.gov.scot/publications/unconventional-oil-gas-understanding-monitoring-induced-seismic-activity/].

Baptie, B., Luckett, R., Butcher, A. & Werner, M.J. (2020). *Robust relationships for magnitude conversion of PNR seismicity catalogues*. British Geological Survey Open Report, OR/20/042. 46pp.

BC Oil and Gas Commission (2012). *Investigation of observed seismicity in the Horn River basin* (Technical report) BC Oil and Gas Comm., Victoria, B. C., Canada. [Available at www.bcogc.ca/node/8046/download.]

Beach, A. (2006). The structure and development of the Lough Allen Basin, N W Ireland. Report for Finavera Gas Ltd. Available from Geological Survey of Northern Ireland as released report PPA279.

Bhattacharya, P., & Viesca, R. C. (2019). Fluid-induced aseismic fault slip outpaces pore-fluid migration. *Science*, 364(6439), 464-468.

Bommer, J.J., Oates, S., Mauricio Cepeda, J., Lindholm, C., Bird, J., Torres, R., Marroquín, G. & Rivas, J. (2006). Control of hazard due to seismicity induced by a hot fractured rock geothermal project. *Engineering Geology*, 83(4), 287-306.

Bommer, J.J., Dost, B., Edwards, B., Stafford, P.J., van Elk, J., Doornhof, D. & Ntinalexis, M. (2016). Developing an application-specific ground-motion model for induced seismicity. *Bulletin of the Seismological Society of America*, 106(1), 158-173.

Brudzinski, M. R., & Kozłowska, M. (2019). Seismicity induced by hydraulic fracturing and wastewater disposal in the Appalachian Basin, USA: A review. Acta Geophysica, 67(1), 351–364. https://doi.org/10.1007/s11600-019-00249-7

Calais, E., Camelbeeck, T., Stein, S., Liu, M., & Craig, T. J. (2016). A new paradigm for large earthquakes in stable continental plate interiors. *Geophysical Research Letters*, 43, 10,621–10,637. https://doi.org/10.1002/2016GL070815.

Cappa, F., Scuderi, M.M., Collettini, C., Guglielmi, Y., & Avouac, J.P. (2019). Stabilization of fault slip by fluid injection in the laboratory and in situ. *Science Advances*, **5**(3). https://doi.org/10.1126/sciadv.aau4065

Chen, H., & Carter, K.E. (2016). Water usage for natural gas production through hydraulic fracturing in the United States from 2008 to 2014. *Journal of Environmental Management*, **170**, 152–159. https://doi.org/10.1016/j.jenvman.2016.0

Clarke, H., Eisner, L., Styles, P., & Turner, P. (2014). Felt seismicity associated with shale gas hydraulic fracturing: The first documented example in Europe. *Geophysical Research Letters*, **41**, 8308–8314. https://doi.org/10.1002/2014GL062047

Clarke, H., Verdon, J.P., Kettlety, T., Baird, A. F., & Kendall, J. M. (2019). Real-time imaging, forecasting, and management of human-induced seismicity at Preston New Road, Lancashire, England. *Seismological Research Letters*, **90**(5), 1902-1915. https://doi.org/10.1785/0220190110.

Cooper, M.R., Anderson, H., Walsh, J.J., Van Dam, C.L., Young, M.E., Earls, G. & Walker, A. (2012). Palaeogene Alpine tectonics and Icelandic plume-related magmatism and deformation in Northern Ireland. *Journal of the Geological Society*, 169, 29–36. https://dx.doi.org/10.1144/0016-76492010-182.

Corlett, H., Schultz, R., Branscombe, P., Hauck, T., Haug, K., MacCormack, K., & Shipman, T. (2018). Subsurface faults inferred from reflection seismic, earthquakes, and sedimentological relationships: Implications for induced seismicity in Alberta, Canada. *Marine and Petroleum Geology*, 93, 135–144. https://doi.org/10.1016/j.marpetgeo.2018.03.008.

Cremen, G., Werner, M.J. & Baptie, B. (2019). A New Procedure for Evaluating Ground-Motion Models, with Application to Hydraulic-Fracture-Induced Seismicity in the United Kingdom.

Bulletin of the Seismological Society of America, 110, 2380-2397, https://doi.org/10.1785/0120190238.

Cremen, G. & Werner, M.J. (2020). A novel approach to assessing nuisance risk from seismicity induced by UK shale gas development, with implications for future policy design. *Natural Hazards and Earth System Sciences*, 20, 2701–2719. https://doi.org/10.5194/nhess-20-2701-2020.

CSA Group Ltd., 2006. Geology of the Lough Allen Basin. Report for Finavera Gas Ltd. Available from Geological Survey of Northern Ireland as released report PPA283.

Darold, A., Holland, A. A., Chen, C., & Youngblood, A. (2014). *Preliminary analysis of seismicity near Eagleton 1–29, Carter County*. Oklahoma Geological Survey Open File Report OF2-2014, Oklahoma Geological Survey.

Davies, R., Foulger, G., Bindley, A. & Styles, P. (2013). Induced seismicity and hydraulic fracturing for the recovery of hydrocarbons. *Marine and Petroleum Geology*, 45, 171-185.

Davison, C., 1924. *History of British Earthquakes*. Cambridge University Press, Cambridge.

Deng, K., Liu, Y., & Harrington, R. M. (2016). Poroelastic stress triggering of the December 2013 Crooked Lake, Alberta, induced seismicity sequence. *Geophysical Research Letters*, **43**, 8482–8491. https://doi.org/10.1002/2016GL070421

de Pater, H. & Baisch, S. (2011). *Geomechanical Study of Bowland Shale Seismicity*. Synthesis Report by StrataGen/Q-con for Cuadrilla Resources Ltd. [Available at www.cuadrillaresources.com/wpcontent/uploads/2012/02/Geomechanical-Study-of-Bowland-Shale-Seismicity_02-11-11.pdf].

Detournay, E. (2016). Mechanics of hydraulic fractures. *Annual Review of Fluid Mechanics*, **48**, 311–339. https://doi.org/10.1146/annurev-fluid-010814-014736.

Douglas, J. & Aochi, H. (2008). A survey of techniques for predicting earthquake ground motions for engineering purposes. *Surveys in Geophysics*, 29(3), 187-220.

Douglas, J., Edwards, B., Convertito, V., Sharma, N., Tramelli, A., Kraaijpoel, D., Mena Cabrera, B., Maercklin, N. & Troise, C. (2013). Predicting ground motions from induced earthquakes in geothermal areas. *Bulletin of the Seismological Society of America*, 103(3), 1875-1897.

Douglas, J. & Edwards, B. (2016). Recent and future developments in earthquake ground motion estimation. *Earth-Science Reviews*, 160, 203-219.

Eaton, D. W., & Schultz, R. (2018). Increased likelihood of induced seismicity in highly overpressured shale formations. *Geophysical Journal International*, 214(1), 751–757. https://doi.org/10.1093/gji/ggy167.

Eaton, D. W., Igonin, N., Poulin, A., Weir, R., Zhang, H., Pellegrino, S., & Rodriguez, G. (2018). Induced Seismicity Characterization during Hydraulic-Fracture Monitoring with a Shallow-Wellbore Geophone Array and Broadband Sensors. *Seismological Research Letters*, *89*(5), 1641–1651. https://doi.org/10.1785/0220180055

Edwards, B., Crowley, H., Pinho, R. & Bommer, J.J. (2021). Seismic Hazard and Risk Due to Induced Earthquakes at a Shale Gas Site. *Bulletin of the Seismolological Society of America*, XX, 1–23, https://doi.org/10.1785/0120200234

Ellsworth, W. L. (2013). Injection-induced earthquakes. *Science*, **341**(6142), 1225942. https://doi.org/10.1126/science.1225942

Ellsworth, W. L., Llenos, A. L., McGarr, A. F., Michael, A. J., Rubinstein, J. L., Mueller, C. S., Petersen, M. D., & Calais, E. (2015). Increasing seismicity in the US midcontinent: Implications for earthquake hazard. *The Leading Edge*, **34**(6), 618–626. https://doi.org/10.1190/tle34060618.1

Ellsworth, W. L., Giardini, D., Townend, J., Ge, S., & Shimamoto, T. (2019). Triggering of the Pohang, Korea, earthquake (Mw 5.5) by enhanced geothermal system stimulation. *Seismological Research Letters*, **90**(5), 1844–1858. https://doi.org/10.1785/0220190102.

Eyre, T. S., Eaton, D. W., Zecevic, M., D'Amico, D., & Kolos, D. (2019a). Microseismicity reveals fault activation before Mw 4.1 hydraulic-fracturing induced earthquake. *Geophysical Journal International*, **218**(1), 534–546. https://doi.org/10.1093/gji/ggz168

Eyre, T. S., Eaton, D. W., Garagash, D. I., Zecevic, M., Venieri, M., Weir, R., & Lawton, D. C. (2019b). The role of aseismic slip in hydraulic fracturing–induced seismicity. *Science advances*, 5(8), eaav7172.

Farahbod, A. M., Kao, H., Cassidy, J. F., & Walker, D. (2015). How did hydraulic-fracturing operations in the Horn River Basin change seismicity patterns in northeastern British Columbia, Canada? *The Leading Edge*, 34(**6**), 658–663. https://doi.org/10.1190/tle34060658.1

Fasola, S. L., Brudzinski, M. R., Skoumal, R. J., Langenkamp, T., Currie, B. S., & Smart, K. J. (2019). Hydraulic fracture injection strategy influences the probability of earthquakes in the Eagle Ford shale play of South Texas. *Geophysical Research Letters*, **46**, 12,958–12,967. https://doi.org/10.1029/2019GL085167

Friberg, P.A., Besana-Ostman, G.M. & Dricker, I. (2014). Characterization of an earthquake sequence triggered by hydraulic fracturing in Harrison County, Ohio. *Seismological Research Letters*, **85**(6), 1295-1307.

Gallegos, T. J. & Varela, B.A. (2014). *Trends in hydraulic fracturing distributions and treatment fluids, additives, proppants, and water volumes applied to wells drilled in the United States from 1947 through 2010: Data analysis and comparison to the literature.* U.S. Geological Survey Science Investigation Report 2014-5131.

Ghofrani, H., & Atkinson, G. M. (2016). A preliminary statistical model for hydraulic fracture-induced seismicity in the Western Canada Sedimentary basin. Geophysical Research Letters, 43, 10,164–10,172. https://doi.org/10.1002/2016GL070042.

Ghofrani, H., & Atkinson, G. M. (2020). Activation rate of seismicity for hydraulic fracture wells in the Western Canada Sedimentary Basin. *Bulletin of the Seismological Society of America*. https://doi.org/10.1785/0120200002

Giardini, D. (2009). Geothermal quake risks must be faced. *Nature*, 462, 848-849.

Goebel, T.H.W., Weingarten, M., Chen, X., Haffener, J. & Brodsky, E.E. (2017). The 2016 Mw5.1 Fairview, Oklahoma earthquakes: Evidence for long-range poroelastic triggering at >40 km from fluid disposal wells. *Earth and Planetary Science Letters*, 472, 50-61.

Goodfellow, S. D., Nasseri, M. H. B., Maxwell, S. C., & Young, R. P. (2015). Hydraulic fracture energy budget: Insights from the laboratory. *Geophysical Research Letters*, **42**, 3179–3187. https://doi.org/10.1002/2015GL063093.

Green, C. A., Styles P. & Baptie, B. J. (2012). *Preese Hall shale gas fracturing review and recommendations for induced seismic mitigation*, Department of Energy and Climate Change [Available at https://www.gov.uk/government/publications/preese-hall-shale-gas-fracturing-review-and-recommendations-for-induced-seismic-mitigation].

Gregory, K. B., Vidic, R. D., & Dzombak, D. A. (2011). Water management challenges associated with the production of shale gas by hydraulic fracturing. *Elements*, **7**(3), 181–186. https://doi.org/10.2113/gselements.7.3.18

Grigoli, F., Cesca, S., Priolo, E., Rinaldi, A.P., Clinton, J.F., Stabile, T.A., Dost, B., Fernandez, M.G., Wiemer, S. & Dahm, T. (2017). Current challenges in monitoring, discrimination, and management of induced seismicity related to underground industrial activities: a European perspective. *Reviews of Geophysics*, 55, 310– 340.

Grünthal, G., (1998). *European Macroseismic Scale 1998*, Cahiers du Centre Européen de Géodynamique et de Séismologie Volume 15, Luxembourg.

Gutenberg, B. & Richter, C.F. (1954). *Seismicity of the Earth and Associated Phenomena*, 2nd ed., Princeton University Press.

Hainzl, S., & Ogata, Y. (2005). Detecting fluid signals in seismicity data through statistical earthquake modeling. *Journal of Geophysical Research Solid Earth*, 110(B5).

Hallo, M., Oprsal, I., Eisner L. & Ali M.Y. (2014). Prediction of magnitude of the largest potentially induced seismic event. *Journal of Seismology*, 18, 421–431.

Healy, J.H., Rubey, W.W., Grigg,s D.T. & Raleigh, C.B. (1968). The Denver earthquakes. *Science*, 161(3848), 1301–1310.

Holland, A. (2013). Earthquakes triggered by hydraulic fracturing in South-Central Oklahoma. *Bulletin of the Seismological Society of America*, 103 (3), 1784-1792. https://doi.org/10.1785/0120120109.

Holschneider, M., G. Zöller, and S. Hainzl (2011), Estimation of the maximum possible magnitude in the framework of a doubly truncated Gutenberg-Richter model. *Bulletin of the Seismological Society of America*, 101(4), 1649–1659, doi:10.1785/0120100289.

Holschneider, M., G. Zoller, R. Clements, and D. Schorlemmer (2014), Can we test for the maximum possible earthquake magnitude? *Journal of Geophysical Research Solid Earth*, 119, 2019–2028, doi:10.1002/2013JB010319.

Hooper, A., Keating, D. & Olsen, R. (2016). *UGEE Integrated Synthesis Report.* Joint Research Programme on the Environmental Impacts of Unconventional Gas Exploration and Extraction, Environmental Protection Agency, Ireland. ISBN: 978-1-84095-701-3. [Available at https://www.epa.ie/pubs/reports/research/ugeejointresearchprogramme/].

Kao, H., Hyndman, R., Jiang, Y., Visser, R., Smith, B., Babaie Mahani, A., Leonard, L., Ghofrani, H., & He, J. (2018). Induced seismicity in western Canada linked to tectonic strain rate: Implications for regional seismic hazard. *Geophysical Research Letters*, **45**, 11–104. https://doi.org/10.1029/2018GL079288.

Kelly, J.G. & Jones, G.Ll. (2020). A revised Mississippian (Courceyan –Chadian) geology of the Clogher Valley, counties Fermanagh and Tyrone (Northern Ireland). *Irish Journal of Earth Sciences*, **38**, 41-71. https://www.jstor.org/stable/10.3318/ijes.2019.38.6.

Keranen, K.M., Weingarten, M. (2018). Induced Seismicity. *Annual Review of Earth and Planetary Sciences*, 46 (1), 149-174.

Kettlety, T., Verdon, J. P., Werner, M. J., & Kendall, J. M. (2019). Stress transfer from opening hydraulic fractures controls the distribution of induced seismicity. *Journal of Geophysical Research: Solid Earth*, **125**, e2019JB018794. https://doi.org/10.1029/2019JB018794

Kozłowska, M., Brudzinski, M. R., Friberg, P., Skoumal, R. J., Baxter, N. D., & Currie, B. S. (2018). Maturity of nearby faults influences seismic hazard from hydraulic fracturing. *Proceedings of the National Academy of Sciences*, **115**(8), E1720 E1729. https://doi.org/10.1073/pnas.1715284115

Kwiatek, G., Saarno, T., Ader, T., Bluemle, F., Bohnhoff, M., Chendorain, M., Dresen, G., Heikkinen, P., Kukkonen, I., Leary, P., Leonhardt, M., Malin, P., Martínez-Garzón, P., Passmore, K., Passmore, P., Valenzuela, S. & Wollin, C. (2019). Controlling fluid-induced seismicity during a 6.1-km-deep geothermal stimulation in Finland. *Science Advances*, 5: eaav7224.

Lee, K.K., Ellsworth, W.L., Giardini, D., Townend, J., Ge, S., Shimamoto, T., Yeo, I.-W., Kang, T.-S., Rhie, J., Sheen, D.-H., Chang, C., Woo, J.-U. & Langenbruch C. (2019). Managing injection-induced seismic risks. *Science,* 364 (6442), 730-732.

Lei, X., Huang, D., Su, J, Jiang, G, Wang, X., Wang, H., Guo, X. & Fu H. (2017). Fault reactivation and earthquakes with magnitudes of up to Mw4.7 induced by shale-gas hydraulic fracturing in Sichuan Basin, China. *Nature Scientific Reports, 7*, 7971. https://doi.org/10.1038/s41598-017-08557-y

Lei, X., Wang, Z. & Su, J. (2019). The December 2018 ML 5.7 and January 2019 ML 5.3 Earthquakes in South Sichuan Basin Induced by Shale Gas Hydraulic Fracturing. *Seismological Research Letters*, 90 (3), 1099–1110. https://doi.org/10.1785/0220190029.

Liang, F., Sayed, M., Al-Muntasheri, G. A., Chang, F. F., & Li, L. (2016). A comprehensive review on proppant technologies. *Petroleum*, **2**(1), 26-39. https://doi.org/10.1016/j.petlm.2015.11.

Majer, E.L., Nelson, J., Tait, A. & Wong, I. (2012). *Protocol for addressing induced seismicity associated with enhanced geothermal systems* (DOE/EE-0662). U.S. Department of Energy Geothermal Technologies Program.

Mancini, S., Werner, M.J., Baptie, B.J. & Segou, M. (2020). *Statistical Modelling and Forecasting of the Preston New Road Seismicity*. British Geological Survey Commissioned Report, CR/20/032. 43pp.

McGarr, A., Simpson, D. & Seeber, L. (2002). Case histories of induced and triggered seismicity. In W.H.K. Lee, H. Kanamori, P.C. Jennings & C. Kisslinger (Eds.), *International Handbook of Earthquake and Engineering Seismology*, (Vol. 81, 647–664). International Association of Seismology and Physics of the Earth's Interior, Academic Press.

McGarr, A. (2014). Maximum magnitude earthquakes induced by fluid injection. *Journal of Geophysical Research*, **119**, 1008-1019. https://doi.org/10.1002/2013JB010597.

Meng, L., McGarr, A., Zhou, L., & Zang, Y. (2019). An investigation of seismicity induced by hydraulic fracturing in the Sichuan basin of China based on data from a temporary seismic network. *Bulletin of the Seismological Society of America*, **109**(1), 348–357. https://doi.org/10.1785/0120180310

Mignan, A., Broccardo, M., Wiemer, S. & Giardini, D. (2017). Induced seismicity closed-form traffic light system for actuarial decision-making during deep fluid injections. *Nature Scientific Reports*, 7, 13607.

Mitchell, W.I. (2004). *The Geology of Northern Ireland—Our Natural Foundation*. Geological Survey of Northern Ireland, W.I. Mitchell (Ed.). Belfast (2004), 318pp.

Myers, T. (2012). Potential contaminant pathways from hydraulically fractured shale to aquifers. *Groundwater*, **50**(6), 872–882. https://doi.org/10.1111/j.1745-6584.2012.00933.x

National Research Council (2012). *Induced seismicity potential in energy technologies*, National Academies Press, Washington D.C.

Palisch, T.T., Vincent, M., & Handren, P.J. (2010). Slickwater fracturing: Food for thought. *SPE Production & Operations*, **25**(03), 327–344. https://doi.org/10.2118/115766-PA.

Pawley, S., Schultz, R., Playter, T., Corlett, H., Shipman, T., Lyster, S., & Hauck, T. (2018). The geological susceptibility of induced earthquakes in the Duvernay play. *Geophysical Research Letters*, 45, 1786–1793. https://doi.org/10.1002/2017GL076100.

Philcox, M.E., Baily, H., Clayton G. & Sevastopulo, G. D. (1992). Evolution of the Carboniferous Lough Allen Basin, Northwest Ireland. *Geological Society, London, Special Publications*, 62, 203-215. https://doi.org/10.1144/GSL.SP.1992.062.01.18.

Raleigh, C.B., Healy, J.H. & Bredehoeft, J.D. (1976). An experiment in earthquake control at Rangley, Colorado. *Science*, 191, 1230–1237. https://doi.org//10.1126/science.191.4233.1230.

Richardson, M. (1975). *Seismicity of Ireland*. Electricity Supply Board, Dublin.

Richter, C.F. (1935). An instrumental earthquake magnitude scale. *Bulletin of the Seismological Society of America*, 25, 1-32.

Royal Society and Royal Academy of Engineering (2012). *Shale Gas Extraction in the UK: A Review of Hydraulic Fracturing* (DES2597). Royal Society and Royal Academy of Engineering, London. [Available at https://royalsociety.org/topics-policy/projects/shale-gas-extraction/report/].

Rubenstein, J.L. & Mahani, A.B. (2015). Myths and facts on wastewater injection, hydraulic fracturing, enhanced oil recovery, and induced seismicity. *Seismological Research Letters*, 86(4), 1060–1067.

Savage, H. M., & Brodsky, E. E. (2011). Collateral damage: Evolution with displacement of fracture distribution and secondary fault strands in fault damage zones. *Journal of Geophysical Research*, 116, B03405. https://doi.org/10.1029/2010JB007665.

Schultz, R., Stern, V., Novakovic, M., Atkinson, G. & Gu, Y.G. (2015). Hydraulic fracturing and the Crooked Lake Sequences: Insights gleaned from regional seismic networks. *Geophysical Research Letters*, 42.

Schultz, R., Wang, R., Gu, Y. J., Haug, K. & Atkinson, G. (2017). A seismological overview of the induced earthquakes in the Duvernay play near Fox Creek, Alberta. *Journal of Geophysical Research*, 122, 492–505.

Schultz, R., Atkinson, G., Eaton, D. W., Gu, Y. J., & Kao, H. (2018). Hydraulic fracturing volume is associated with induced earthquake productivity in the Duvernay play. *Science*, 359(6373), 304–308. https://doi.org/10.1126/science.aao0159.

Schultz, R., Skoumal, R. J., Brudzinski, M. R., Eaton, D., Baptie, B., & Ellsworth, W. (2020). Hydraulic Fracturing-Induced Seismicity. *Reviews of Geophysics*, *58*(3). https://doi.org/10.1029/2019RG000695.

Schultz, R., & Wang, R. (2020). A newly emerging case of hydraulic fracturing induced seismicity in the Duvernay East Shale Basin. *Tectonophysics*, 779. https://doi.org/10.1016/j.tecto.2020.228393.

Segall, P. & Lu, S. (2015). Injection-induced seismicity: Poroelastic and earthquake nucleation effects. *Journal of Geophysical Research*, 120, 5082–5103.

Shapiro, S. A., Dinske, C., Langenbruch, C. & Wenzel, F. (2010). Seismogenic index and magnitude probability of earthquakes induced during reservoir fluid stimulations. *The Leading Edge*, **29**, 304–309.

Shen, L. W., Schmitt, D. R., & Schultz, R. (2019). Frictional stabilities on induced earthquake fault planes at Fox Creek, Alberta: A pore fluid pressure dilemma. *Geophysical Research Letters*, 46, 8753–8762. https://doi.org/10.1029/2019GL083566.

Shemeta, J. E., Brooks, C. E., & Lord, C. C. (2019). Well stimulation seismicity in Oklahoma: Cataloging earthquakes related to hydraulic fracturing. In *Unconventional Resources Technology Conference (URTEC)*, (95–106). Brisbane, Australia: Society for Exploration Geophysicists.

Sibson, R. H. (2020). Dual-driven fault failure in the lower seismogenic zone. *Bulletin of the Seismological Society of America*, 110. https://doi.org/10.1785/0120190190.

Silva, V., Crowley, H., Pagani, M., Monelli, D., Pinho, R. (2014). Development of the OpenQuake engine, the Global Earthquake Model's open-source software for seismic risk assessment, *Natural Hazards*, 72 (3), 1409–1427.

Skoumal, R.J., Brudzinski, M.R. & Currie, B.S. (2015a). Earthquakes induced by hydraulic fracturing in Poland Township, Ohio. *Bulletin of the Seismological Society of America*, **105**(1), 189–197.

Skoumal, R.J., Brudzinski, M.R., & Currie, B.S. (2015b). Distinguishing induced seismicity from natural seismicity in Ohio: Demonstrating the utility of waveform template matching. *Journal of Geophysical Research: Solid Earth*, **120**, 6284–6296. https://doi.org/10.1002/2015JB012265

Skoumal, R.J., Ries, R., Brudzinski, M.R., Barbour, A.J., & Currie, B.S. (2018a). Earthquakes induced by hydraulic fracturing are pervasive in Oklahoma. *Journal of Geophysical Research: Solid Earth*, **123**, 10,918–10,935. https://doi.org/10.1029/2018JB016790.

Skoumal, R. J., Brudzinski, M. R., & Currie, B. S. (2018b). Proximity of Precambrian basement affects the likelihood of induced seismicity in the Appalachian, Illinois, and Williston Basins, central and eastern United States. *Geosphere*, 14(3), 1365–1379. https://doi.org/10.1130/GES01542.1.

Skoumal, R.J., Barbour, A.J., Brudzinski, M.R., Langenkamp, T., & Kaven, J.O. (2020). Induced seismicity in the Delaware Basin, Texas. *Journal of Geophysical Research: Solid Earth*, **125**, e2019JB018558. https://doi.org/10.1029/2019JB018558

Utsu, T. (1961). A statistical study on the occurrence of aftershocks. *The Geophysical Magazine*, 30, 521-605.

Van der Elst, N. J., Page, M. T., Weiser, D. A., Goebel, T. H., & Hosseini, S. M. (2016). Induced earthquake magnitudes are as large as (statistically) expected. *Journal of Geophysical Research: Solid Earth*, **121**, 4575–4590. https://doi.org/10.1002/2016JB012818

Verdon, J. P. & Budge, J. (2018). Examining the capability of statistical models to mitigate induced seismicity during hydraulic fracturing of shale gas reservoirs. *Bulletin of the Seismological Society of America*, 108, 690–701.

Walsh, F.R. III & Zoback, M.D. (2016). Probabilistic assessment of potential fault slip related to injection-induced earthquakes: Application to north-central Oklahoma, USA. *Geology*, **44**(12), 991–994.

Weichert, D. H. (1980). Estimation of the earthquake recurrence parameters for unequal observation periods for different magnitudes. *Bulletin of the Seismological Society of America*, 70, 1337–1346.

Worthington, R.P. & Walsh, J.J. (2011). Structure of Lower Carboniferous basins of NW Ireland, and its implications for structural inheritance and Cenozoic faulting. *Journal of Structural Geology*, 33, 1285–99

Yoon, C., Huang, Y., Ellsworth, W.L. & Beroza, G.C. (2017). Seismicity during the initial stages of the Guy-Greenbrier, Arkansas, earthquake sequence. *Journal of Geophysical Research*: Solid Earth, 122, 9253–9274.

Yu, H., Harrington, R. M., Liu, Y., & Wang, B. (2019). Induced seismicity driven by fluid diffusion revealed by a near-field hydraulic stimulation monitoring array in the Montney Basin, British Columbia. *Journal of Geophysical Research: Solid Earth*, 124, 4694–4709. https://doi.org/10.1029/2018JB017039.